Supporting Information

Excitation Dependent Electron Exchange Energy and Electron Transfer Dynamics in a Series of Covalently Tethered *N, N*-bis (4′-*tert*-butylbiphenyl-4-yl) aniline - [C_{60}] Fullerene Dyads *via* varying π-conjugated Spacers

Suneel Gangada[a], Madhu Chakali [bd], Haraprasad Mandal[bd], Naresh Duvva[c], Raghu Chitta[ae*] Lingamallu Giribabu [cd*], Prakriti Ranjan Bangal[bd*]

a. Department of Chemistry, Central University of Rajasthan, Bandarsindri, Tehsil: Kishangarh, Dist. Ajmer, Rajasthan – 305817, India.
b. Analytical Division, CSIR- Indian Institute of Chemical Technology, Uppal Road, Tarnaka, Hyderabad, 500007, India.
c. Polymers & Functional Materials Division, CSIR- Indian Institute of Chemical Technology, Uppal Road, Tarnaka, Hyderabad, 500007, India
d. Academy of Scientific and Innovative Research, AcSIR, New Delhi.
e. Present address: Department of Chemistry, National Institute of Technology Warangal, Hanamkonda, Warangal - 506004.Telangana, India

*Corresponding Author(s): prakriti@iict.res.in; raghuchitta@nitw.ac.in; giribabu@iict.res.in

Supporting Information

Synthesis Details:

1. *N, N*-bis (4′-*tert*-butylbiphenyl-4-yl)aniline) (BBA) (1). To a schlenk flask was added 4-bromo-4-*tert*-butylbiphenyl (2 g, 6.91 mmol), NaO^tBu (828 mg, 8.62 mmol), $Pd(dba)_2$ (18.88 mg, 0.03mmol), dppf (27.15 mg, 0.04 mmol), and dry toluene (40 mL) under inert atmosphere. Then aniline (322 mg 3.45 mmol) was added and the reaction mixture was refluxed for 14 h. After completion of the reaction, the reaction mixture was poured into water and extracted with diethyl ether. The organic layer was dried over sodium sulfate and the compound was isolated by silica gel column chromatography using hexane: toluene (70:30 v/v) as an eluent. Yield: 1.39 g (79%). ^{1}H NMR ($CDCl_3$, 500 Hz): δ 7.52-7.44 (m, 12 H), 7.28-7.25 (m, 2H), 7.17 (d, *J* = 6.5 Hz, 6H), 7.04 (t, *J* = 7.5 Hz, 1H), 1.36 (s, 18H).^{13}C NMR ($CDCl_3$, 125 Hz): 31.42, 34.54, 123.02, 124.18, 124.59, 125.72, 126.36, 127.71, 129.34, 135.29, 137.87, 146.79, 147.66, 149.83.MALDI-TOF: (m/z) found 510.12 (M^+, $C_{38}H_{39}N$ requires 509.31)

2. *N, N*-bis(4′-*tert*-butylbiphenyl-4-yl)4-bromoaniline(2). To a solution of compound **1** (100 mg, 0.19 mmol), was added *N*-bromosuccinamide (41 mg, 0.23 mmol), in $CHCl_3$ under inert atmosphere. After 6 h, the reaction mixture was quenched with water and extracted using chloroform. Organic layer was dried over sodium sulfate and the desired compound was isolated by using silica gel column chromatography using hexane: toluene (90:10 v/v) as an eluent. Yield: 102 mg (92%). ^{1}H NMR ($CDCl_3$, 500 Hz): δ 7.53-7.45 (m, 12H), 7.37 (d, *J* = 8.5Hz, 2H), 7.16 (d, *J* = 9Hz, 4H), 7.05 (d, *J* = 9Hz, 2H), 1.37 (s, 18H). MALDI-TOF: (m/z) found 589 (M^+, $C_{38}H_{38}BrN$ requires 587.22)

3. 4-(Bis(4′-*tert*-butylbiphenyl-4-yl)amino)benzaldehyde(3). To 5 mL of DMF was added 1 mL of $POCl_3$ (0.842 g, 5.49 mmol) at 0°C and stirred for 1 h. To the Vilsmeier reagent was added a solution of **1** (0.4 g, 0.79mmol) in 10 mL of DMF at 0°C and heated at 80°C for 4 h. After the reaction mixture was cooled to room temperature, it was poured into 1 L of 2% w/v NaOH aqueous solution and extracted with ether. The organic layer was dried over Na_2SO_4 and concentrated *in vacuo* to give the crude product. The purified product was isolated as an yellow solid by silica gel column chromatography using toluene as eluent.Yield: 253 mg(60%). ^{1}H NMR ($CDCl_3$, 500 Hz): δ 9.83 (s, 1H), 7.72 (d, *J*=8 Hz, 2H), 7.58-7.53 (m, 8H), 7.47 (d, *J* = 8.5 Hz, 4H), 7.26(d, *J* = 7.5 Hz, 4H), 7.14 (d, *J* = 5.5 Hz, 2H), 1.37 (s, 18H).^{13}C NMR ($CDCl_3$, 125 Hz):31.38, 34.58, 119.88, 125.83, 126.35, 126.54, 128.20, 129.34, 131.39, 137.37, 137.76, 145.07, 150.38, 153.22, 199.51 FTIR (KBr , cm^{-1}) 2958 υ (C-H), 1702 υ (C=O), 1498 υ (C=C), 834 υ (C-H)MALDI-TOF: (m/z) found 538.02 (M^+, $C_{39}H_{39}NO$ requires 537.30).

4. 4′-(Bis(4′-*tert*-butylbiphenyl-4-yl)amino)biphenyl-4-carbaldehyde (4). 2 (300 mg, 0.51 mmol), 4-formylphenylboronic acid (91.70 mg, 0.61mmol), $Pd(PPh_3)_2Cl_2$ (35 mg, 0.03 mmol), PPh_3 (30 mg, 0.03 mmol), and K_2CO_3 (176 mg, 1.24 mmol) were added to a Schlenkflask. 30 mL of THF: H_2O (4:1 v/v) was added under nitrogen atmosphere and the reaction mixture was heated and stirred overnight at 90°C. After the reaction was completed, CH_2Cl_2 was added and the reaction mixture was washed with water and the organic layer was dried over sodium sulfate. The crude product was purified by silica gel column chromatography using hexane: dichloromethane (70:30 v/v) to afford the product as a yellow powder. Yield: 203 mg (65%). ^{1}H NMR ($CDCl_3$, 500 Hz): δ 10.04 (s, 1H), 7.94 (d, *J* = 8 Hz, 2H), 7.75 (d, *J* = 8 Hz, 2H), 7.57-7.52 (m, 11H), 7.46 (d, *J* = 8.5 Hz, 4H), 7.26-7.22 (m, 5H), 1.36 (s, 18H).^{13}C NMR ($CDCl_3$, 125 Hz):31.40,34.56, 123.58, 124.89, 125.77, 126.41, 126.96, 127.89, 128.14, 130.39, 133.11, 134.73, 136.09, 137.64, 146.24, 146.62, 148.21, 150.04, 191.90. FTIR (KBr , cm^{-1}) 2950 υ (C-H), 1698 υ (C=O), 1586 υ (C=C), 832 υ (C-H).MALDI-TOF: (m/z) found 614.28 (M^+, $C_{45}H_{43}NO$ requires 613.33).

5. 4-(4-(Bis (4′-*tert*-butylbiphenyl-4-yl)amino)phenylethynyl)benzaldehyde(5). 2 (300 mg, 0.510 mmol), 4-ethynylbenzaldehyde (171.21 mg, 1.3 mmol), $Pd(PPh_3)_2Cl_2$ (22 mg, 0.03mmol), PPh_3 (51 mg, 0.03 mmol) and copper(I)iodide (18.45 mg, 0.19 mmol)) were added to a Schlenkflask. Triethylamine (30 mL) was added under nitrogen atmosphere and the reaction mixture was heated and stirred for 48 hours at 90°C. After the reaction was completed, CH_2Cl_2 was added and the reaction mixture was washed with water and the organic layer was dried over sodium sulfate. The crude product was purified by silica gel column chromatography using hexane: dichloromethane (70:30 v/v) to afford the titled product as a yellow powder. Yield: 178 mg (55%).^{1}H NMR ($CDCl_3$, 500 Hz): δ 10.01 (s, 1H), 7.85 (d, *J* = 8.5 Hz, 2H), 7.65 (d, *J* = 8 Hz, 2H), 7.54-7.52 (m, 8H), 7.47-7.42 (m, 6H), 7.21 (d, *J* = 8.5 Hz, 4H), 7.11(d, *J* = 9Hz,2H), 1.36 (s, 18H). ^{13}C NMR ($CDCl_3$, 125 Hz): 31.38, 34.54, 88.11, 94.21, 115.21, 120.19, 122.28, 125.25, 125.75, 126.42, 127.93, 129.60, 131.89, 132.88, 135.12, 136.50, 137.56, 145.90, 148.39, 150.12, 191.42. FTIR (KBr, cm^{-1}) 2949 υ (C-H), 1701 υ (C=O), 1497 υ (C=C), 825 υ (C-H).MALDI-TOF: (m/z) found 638.28 (M^+, $C_{47}H_{43}NO$ requires 637.33).

6. *N*-Methyl-2-(4-(bis(4′-tert-butylbiphenyl-4-yl)amino)phenyl)-3,4-fullero[60]pyrrolidine(Dyad-1) (6). To a solution of C_{60} (100 mg, 0.14mmol) dissolved in toluene (50 mL), sarcosine (40 mg, 0.42mmol), and **3** (373 mg, 0.7 mmol) was added and the reaction mixture was refluxed for 1 h. The reaction mixture was then cooled to room temperature and the solvent was evaporated. The compound was purified by silica gel column chromatography using

hexane: toluene (90:10 v/v).Yield: 53 mg (30%). ^{1}H NMR ($CDCl_3$, 500 Hz): δ 7.73 (s, 2H), 7.49 (d, *J* = 8.5 Hz, 4H), 7.44 (d, *J* = 8.5 Hz, 8H), 7.20 (s, 2H), 7.10 (d, *J* = 8.5 Hz, 4H), 4.98 (s, 1H), 4.27 (d, *J* = 9.5Hz, 1H), 2.88 (s, 3H), 1.34 (s, 18H). ^{13}C NMR ($CDCl_3$, 125 Hz): 31.39, 34.52, 40.13, 69.00, 70.05, 83.13, 124.27, 125.71, 126.34, 127.72, 131.38, 135.47, 136.59, 136.73, 137.68, 139.30, 139.93, 140.14, 140.19, 141.66,141.69, 141.85, 142.07, 142.12, 142.19, 142.29, 142.31, 142.60, 142.64, 142.71, 143.07, 143.21, 144.42, 144.71, 144.74, 145.18, 145.24, 145.29, 145.33, 145.36, 145.50, 145.58, 145.82, 145.97, 145.98, 146.14, 146.19, 146.24, 146.33, 146.42, 146.50, 146.55, 146.91, 147.35, 147.77, 149.87, 153.50, 153.72, 154.07, 156.36. FTIR (KBr, cm^{-1}) 2950 υ (C-H), 1498 υ (C=C), 822 υ (C-H).MALDI-TOF: (m/z) found 1286 (M^+, $C_{101}H_{44}N_2$ requires 1285.44).

7. *N*-Methyl-2-(4′-(bis(4′-*tert*-butylbiphenyl-4-yl)amino)biphenyl-4-yl)-3,4-fullero[60]pyrrolidine (Dyad-2) (7).To a solution of C_{60} (100 mg, 0.138 mmol) dissolved in toluene (50 mL), sarcosine (40 mg, 0.42 mmol), and **4** (425 mg, 0.694 mmol) was added, and the mixture was refluxed for1.5h. The reaction mixture was cooled to room temperature and the solvent was evaporated. The compound was purified by silica gel column chromatography using hexane: toluene (95:5 v/v). Yield: 52 mg (28%). ^{1}H NMR ($CDCl_3$, 500 Hz): δ 7.78 (s, 2H), 7.67 (d, *J* = 8.5Hz, 2H), 7.56(d, *J* = 8.5Hz, 2H), 7.53-7.49 (m, 8H), 7.45(d, *J* = 8.5Hz, 4H), 7.23-7.11 (m, 6H), 4.94 (d, *J* = 9.5Hz, 1H), 4.91 (s, 1H), 4.41 (d, *J* = 9.5Hz, 1H), 2.78 (s, 3H), 1.28 (s, 18H).^{13}C NMR ($CDCl_3$, 125 Hz) 31.39,34.52, 40.11, 69.08, 70.07, 83.43, 124.39, 125.71, 126.35, 127.75, 128.80, 129.79, 134.63, 135.57, 135.77, 135.86, 136.62, 136.91, 137.71, 139.60, 139.93, 140.17, 140.21, 140.50, 141.56, 141.71, 141.89, 141.98, 142.04, 142.07, 142.13, 142.18, 142.27, 142.31, 142.57, 142.60, 142.71, 143.01, 143.12, 143.17, 144.42, 144.63, 144.73, 145.19, 145.26, 145.30, 145.34, 145.37, 145.48, 145.53, 145.57, 145.81, 145.95, 146.13, 146.17, 146.19, 146.25, 146.30, 146.34, 146.52, 146.80, 147.15, 147.33, 149.90, 153.45, 154.05. FTIR (KBr , cm^{-1}) 2947 υ (C-H), 1598 υ (C=C), 818 υ (C-H); MALDI-TOF: (m/z) found1361.96 (M^+, $C_{107}H_{48}N_2$ requires 1361.54).

8. *N*-Methyl-2-(4-(4-(bis(4′-*tert*-butylbiphenyl-4-yl)amino)phenylethynyl)phenyl-3,4-fullero[60]pyrrolidine (Dyad-3) (8). To a solution of C_{60} (100 mg, 0.14mmol) dissolved in toluene (50 mL), sarcosine (40 mg, 0.42 mmol), and**5** (442 mg, 0.7mmol) was added, and the mixture was refluxed for 1 h. The reaction mixture was cooled to room temperature and the solvent was evaporated. The compound was purified by silica gel column chromatography using hexane: toluene (95:5 v/v).Yield: 49 mg (26%). ^{1}H NMR ($CDCl_3$, 500 Hz): δ 7.82(s, 2H), 7.71 (d, *J* = 9Hz, 2H),7.60-7.25 (m, 12H), 7.19(d, *J* = 8 Hz, 2H),7.14 (d, *J* = 9 Hz, 4H),7.09(d, *J* = 9Hz, 2H), 4.99 (d, *J* = 9.5Hz,

1H), 4.95 (s, 1H), 4.27 (d, *J* = 9Hz, 1H), 2.82 (s,3H), 1.36 (s,18H). FTIR (KBr , cm^{-1}) .2947 υ (C-H), 1598 υ (C=C), 818 υ (C-H).MALDI-TOF: (m/z) found 1385.45 (M+, $C_{109}H_{48}N_2$ requires 1385.56).

9. *N*-Methyl-2-phenyl-3,4-fullero[60]pyrrolidine (C_{60}-Ph)(9). To a solution of C_{60} (100 mg, 0.14mmol) dissolved in toluene (50 mL), sarcosine (40 mg, 0.416 mmol) and benzaldehyde (736 mg, 0.693 mmol) was added, and the reaction mixture was refluxed for 1 h. The reaction mixture was cooled to room temperature and the solvent was evaporated. The compound was purified by silica gel column chromatography using hexane: toluene (95:5 v/v) as eluent. Yield: 30.64 mg (26%). ^{1}H NMR ($CDCl_3$, 500 Hz): δ 7.81(s, 2H), 7.43 (t, *J* = 6.5Hz, 2H), 7.34(d, *J* = 7 Hz, 1H), 4.99 (d, *J* = 9 Hz, 1H), 4.94 (s, 1H), 4.27 (d, *J* = 9Hz, 1H), 2.81(s, 3H). (m/z) found 854 (M^+, $C_{69}H_{11}N$ requires 853.83).

Experimental Detail

1. Materials. Commercially available reagents and chemicals were procured from Sigma-Aldrich, SpectrochemCDH and Merck. Analytical reagent (AR) grade solvents were used for the reactions while laboratory reagent (LR) grade solvents were used for purifications and column chromatography. Spectroscopic grade Toluene and *N,N*-dimethylformamide (DMF) were purchased from Sigma-Aldrich and used as received for spectroscopic investigations. Dichloromethane and chloroform were dried in presence of calcium hydride under nitrogen atmosphere. Hexane and toluene was purified by Na metal added benzophenone refluxing overnight, then distilled under vacuum and stored over 4Å molecular sieves. Triethylamine was distilled over NaOH pellets. ACME silica gel (100-200 mesh) was used for column chromatography. Thin-layer chromatography was performed on Merck-precoated silica gel 60-F254 plate. Either gravity or flash chromatography was performed for purification of all compounds. All the reactions were carried out under nitrogen or argon atmosphere using dry and degassed solvents. Synthesis details are given in supplementary information.

2. Methods and Instrumentation.

2.1. General. ^{1}H-NMR spectra were recorded on a 500 MHz Bruker spectrometer. The optical absorption spectra were recorded on Agilent (Cary 100 UV-vis, UV1106M034) spectrophotometer. Steady-state fluorescence spectra were recorded by Fluorolog-3 spectrofluorometer of Horiba JobinYvon, USA.

2.2 Computational Studies. All calculations have been carried out using a Gaussian 09 package using high-speed personal computers.[1] The ground state geometries of all three dyads were optimized to genuine global minimum using B3LYP hybrid function,[2] and 6-31G(d,p) basis set[3] was used as input for further calculations. Frontier molecular orbitals (FMOs) were calculated by Density Functional Theory (DFT) in gas phase.The excited state properties in the dyads were calculated using TD-DFT B3LYP 6-31G (d,p) basis set with the framework of the polarizable continuum model (PCM) in toluene as solvent. The theoretical absorption spectra of the dyads has been computed using the GaussSum software.

2.3 Fluorescence Up-conversion and Transient Absorption

The detail experimental setup of the femtosecond fluorescence up-conversion and transient absorption (TA) measurements is described elsewhere.[4]In brief; fluorescence up-conversion study was performed using FOG 100-DX system (CDP System Corp. Moscow, Russian Federation). The second harmonic of the fundamental beam (~500 mW at 800 nm) of femtosecond oscillator (Mai Tai HP, Spectra Physics, FWHM=100fs) was used as pump and residual of fundamental pulses served as gate beams. A neutral density (ND) filter is used to adjust the power of the excitation beam. The gate beam was directed to gold-coated retro-reflector mirror connected to 8 ns optical delay line before being focused together with the fluorescence (collected by an achromatic doublet, f=80 mm) on 0.5 mm type-I BBO crystal. The angle of the crystal was adjusted to phase matching conditions at the fluorescence wavelength of interest. The intensity of the up-converted radiation was detected through monochromator (CDP2022D) coupled with a photomultiplier tube operating in the photon counting mode. Proper filters were used before the detector to eliminate parasitic light from the up-converted signal if any. The polarization of the excitation pulses was set at magic angle relative to that of the gate pulses using Berek's variable wave plate. The sample solutions were placed in a 0.6 mm or 1 mm rotating cell and absorbance of about ~0.4 at excitation wavelength generally used (yielding a concentration around 100-200 μM). The FWHM of the instrument response function (IRF) in this setup was calculated about 240 fs in the 0.6 mm cell and 260 fs in the 1 mm cell. For data analysis, the fluorescence time profile at a given emission wavelength $I(\lambda,t)$ was reproduced by the convolution of a Gaussian IRF with a sum of exponential trial function representing the pure sample dynamics $S(t)$.

Femtosecond transient absorption studies were performed with a commercial femtosecond Ti:sapphire regenerative amplifier (Spitfire, Laser Spectra) laser system equipped with a CDP transient absorption spectrometer and automated data acquisition system (CDP System Corporation, ExciPro). The regenerative amplifier (Spitfire Ace, Spectra Physics) was seeded with the 100 fspulse (~80 MHz, repetition rate) from the oscillator (Spectra Physics, Maitai), the amplified 100 fs output pulse with 1kHz repetition rate was seeded to optical parametric amplifier (TOPAS prime), and the output of TOPAS was used as pump sources at required wavelength and fed into a spectrometer through a synchronized chopper for 1 kHz repetition rate. A lens (f= 200 mm) was used to adjust the pump diameter while an iris and neutral density filter combination were used to adjust the pump energy. A Berek's variable wave plate was placed in the pump beam and polarization

was fixed at the magic angle with respect to the probe beam. A suitable fraction of the output of the Ti:sapphire regenerative amplifier (at 800 nm) was focused onto a thin rotating CaF2 crystal (prdominently for Uv-vis) or Sapphir crystal (predominantly for Vis-IR) window for generating white light continuum, which then was spitted into two identical fraction making as probe and references beams. After passing through the rotating sample cellprobe and references beams are collectedby two optical fibres, which are connected to the entrance slit of the imaging spectrometer (CDP2022i) which isequipped with UV−vis photodiode (Si linear photodiode) arrays and IR photodiode (GaAs linear photodiode) arrays with spectral response ranges 200−1000 and 900−1700 nm, respectively. Quartz cells of 1 or 2 mm sample path length were used for all studies and IRF was estimated to be ≤125 fs. To minimize the solvent signal pump pulse energy was kept below 3 μJ and probe pulse energy was from 0.1-0.5μJ at the sample. For transient absorption spectra the group velocity dispersion compensation of white light continuum (probe beam) was done using studied solvent's two photon absorption data for few ps delay. All the samples were checked before and after taking the transient absorption to monitor the sample degradation if any.

2.4. Transient Data and Global Analysis

To obtain a model-based description in estimating rate constants and species related spectral signature, the transient data reported in this paper were also analyzed using a singular value decomposition based global and target analysis.[5]The minimum number of components involved in the evolution of transient data was determined globally. Global analysis was performed in two different approaches based on superposition principle of least number of independent exponential components which provided a straightforward description of the data at all measured wavelengths at all time points simultaneously. The numbers of independent components fitted to all data are determined by gradually increasing the number of exponential components until the residuals were effectively reduced to zero. First, the simplest description in global analysis used parallel kinetic model where a number of monoexponentially decaying independent components, each represented by a single rate constant (reciprocal of the lifetime of the corresponding state) and amplitude at each recorded wavelength, yields the decay associated difference spectra. The decay associated difference spectra contemplate the rise and decay of the components with their corresponding decay constants, lifetime values. Second, a sequential kinetic model, namely anunbranched, unidirectional model, consisted of successive monoexponential decays with increasing time constants estimates gross spectral evolution of the

data generating evolution associated difference spectra. Finally, data are fitted to a full kinetic model (compartmental scheme), target analysis, which includes all possible branching routes and equilibrium between compartments specifying the microscopic rate constants that describe the decay of the compartments as well as transfer of excitation between the compartments. This analysis estimates the real spectra of each compartment (excited species) and is termed as species associated difference spectra (SADS). The whole global and target analysis was performed with the R package TIMP and its graphical user interface of Glotaran[6]

Figures and Tables

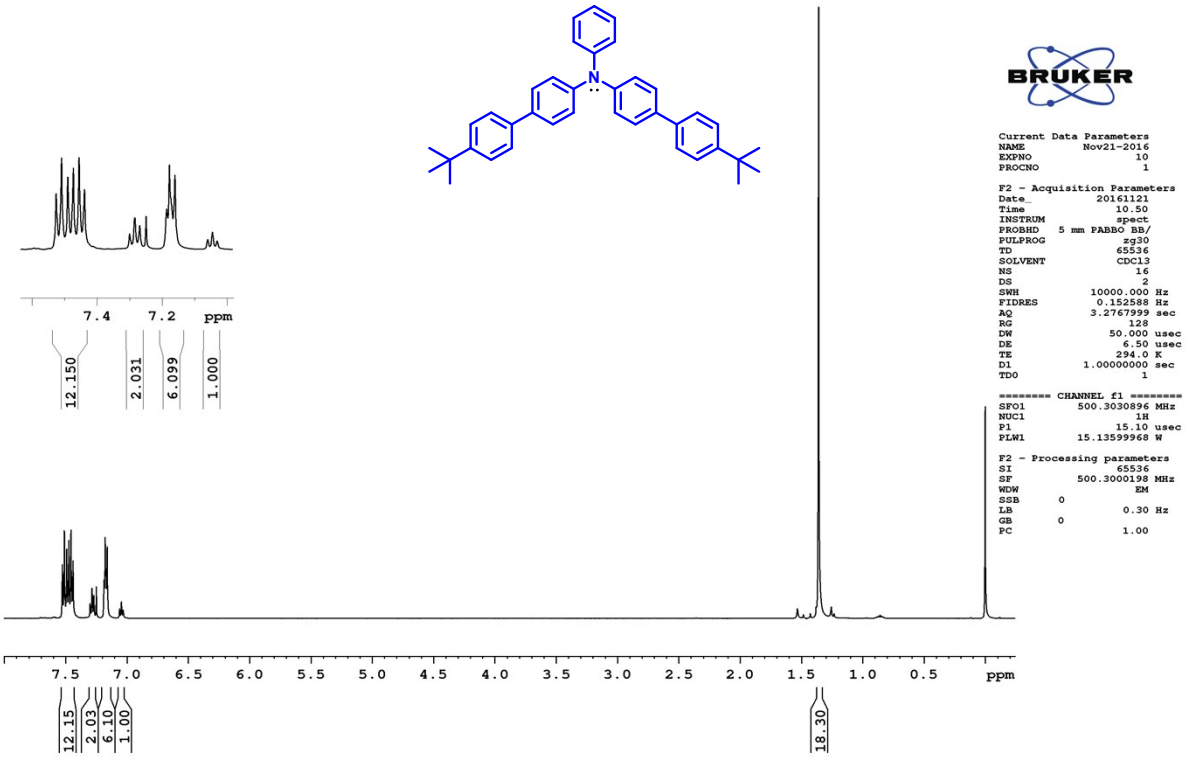

Fig. S1. ^{1}H NMR spectrum of *N, N*-bis (4′-*tert*-butylbiphenyl-4-yl)aniline)**(1)**in $CDCl_3$.

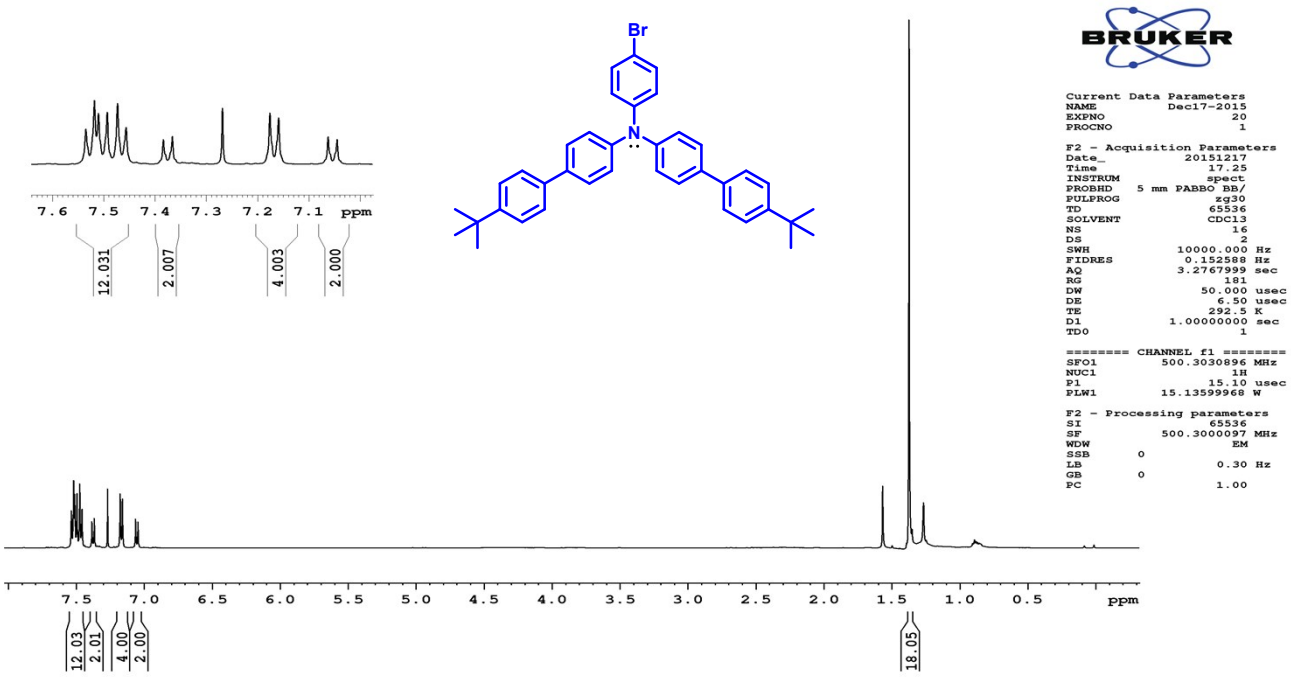

Fig. S2. ^{1}H NMR spectrum of *N, N*-bis(4′-*tert*-butylbiphenyl-4-yl)4-bromoaniline**(2)**in $CDCl_3$.

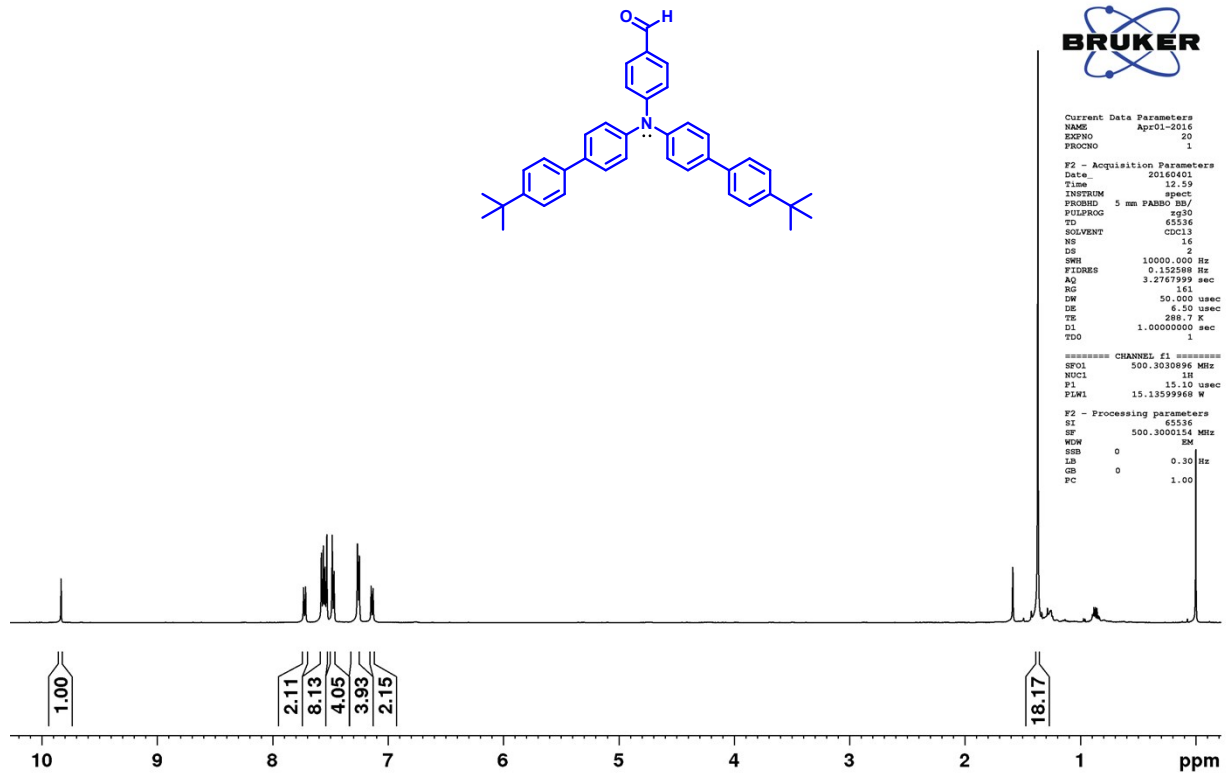

Fig. S3. ^{1}H NMR spectrum of 4-(Bis(4′-*tert*-butylbiphenyl-4-yl)amino)benzaldehyde**(3)**in $CDCl_3$.

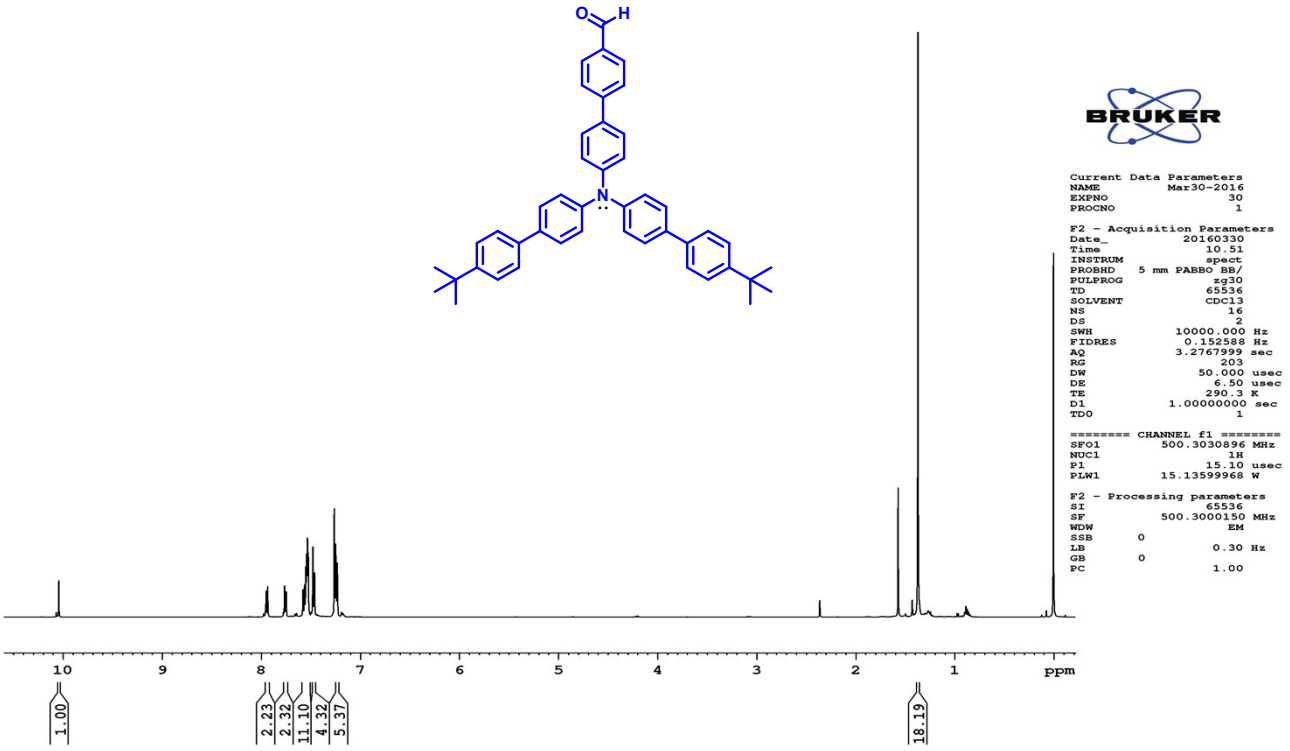

Fig. S4. ^{1}H NMR spectrum of 4′-(Bis(4′-*tert*-butylbiphenyl-4-yl)amino)biphenyl-4-carbaldehyde**(4)**in $CDCl_3$.

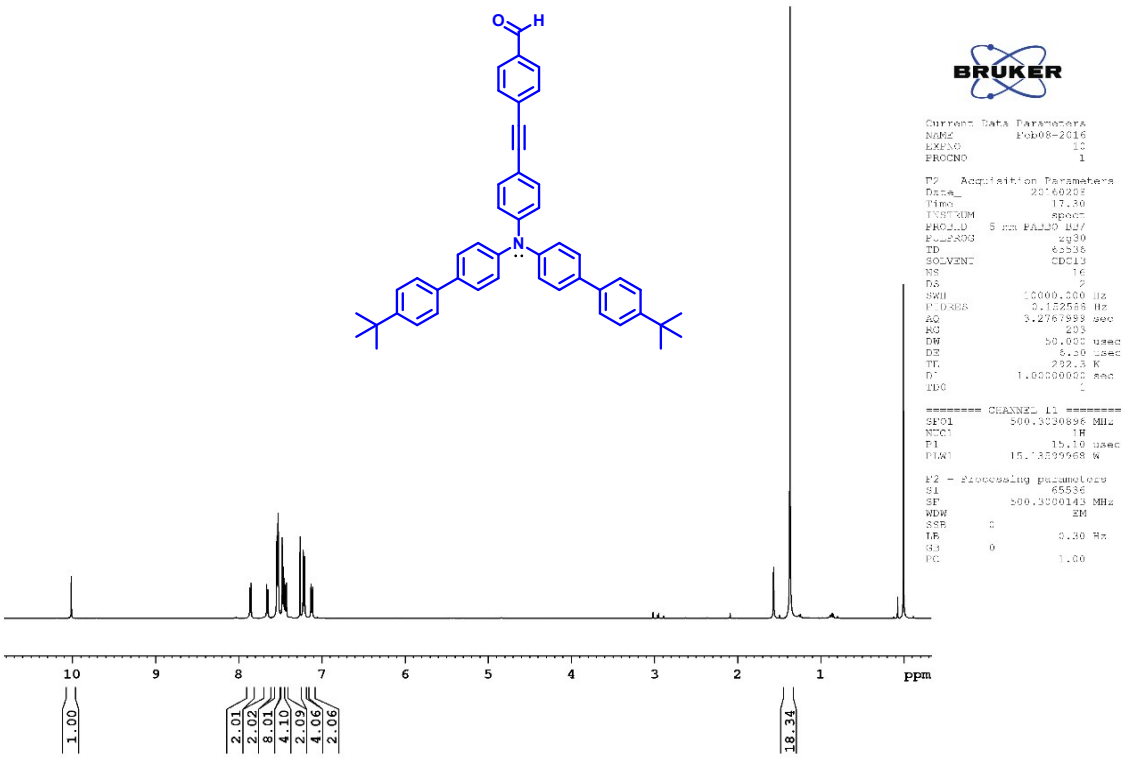

Fig. S5. ^{1}H NMR spectrum of 4-(4-(Bis (4′-*tert*-butylbiphenyl-4-yl)amino)phenylethynyl)benzaldehyde **(5)** in $CDCl_3$.

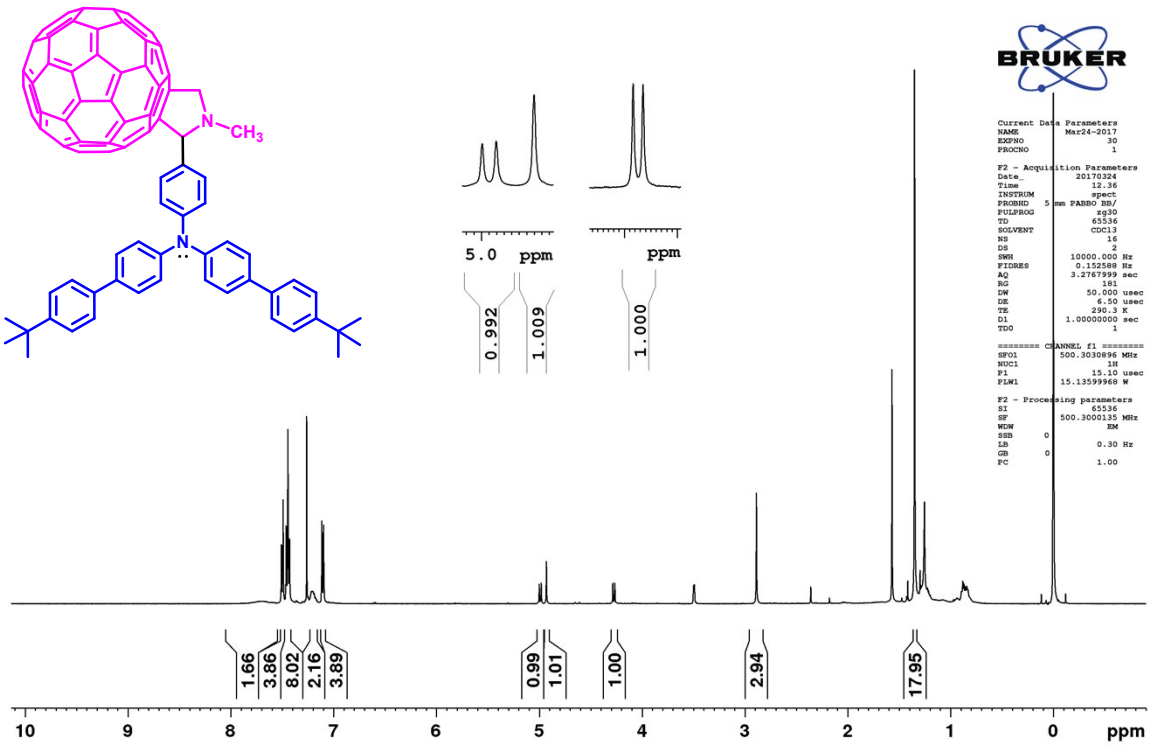

Fig. S6. ^{1}H NMR spectrum of*N*-Methyl-2-(4-(bis(4′-tert-butylbiphenyl-4-yl)amino)phenyl)-3,4-fullero[60]pyrrolidine **(6)** in $CDCl_3$.

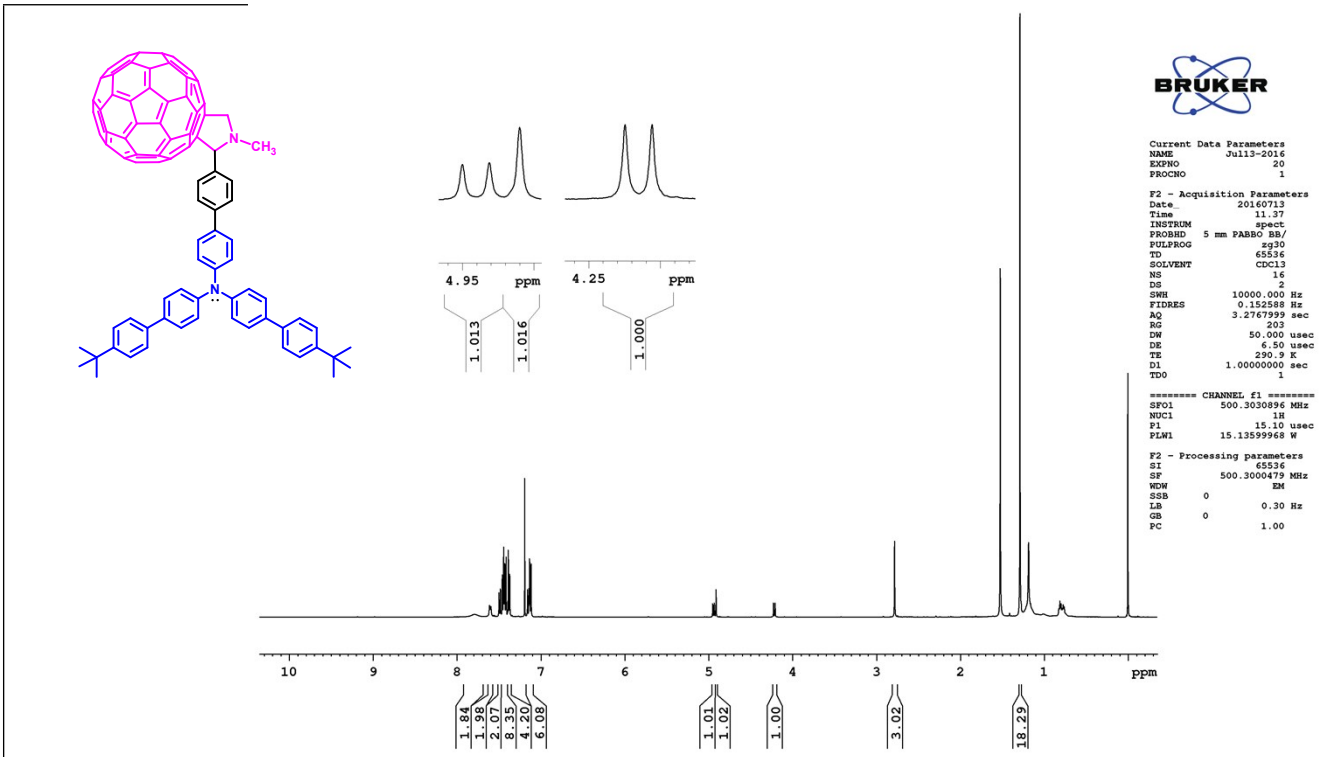

Fig. S7. ^{1}H NMR spectrum of *N*-Methyl-2-(4′-(bis(4′-*tert*-butylbiphenyl-4-yl)amino)biphenyl-4-yl)-3,4-fullero[60]pyrrolidine **(7)** in $CDCl_3$.

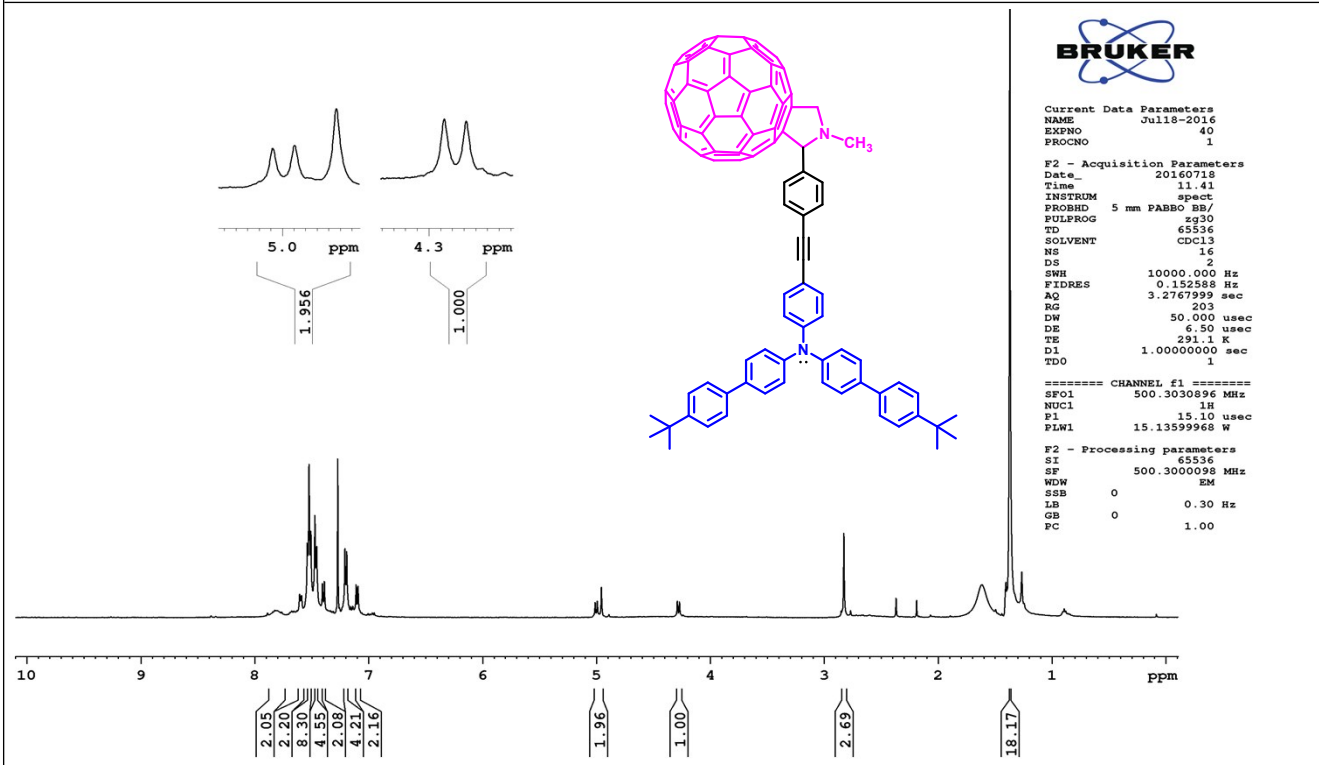

Fig. S8. ^{1}H NMR spectrum of *N*-Methyl-2-(4-(4-(bis(4′-*tert*-butylbiphenyl-4-yl)amino)phenylethynyl)phenyl-3,4-fullero[60]pyrrolidine**(8)** in $CDCl_3$.

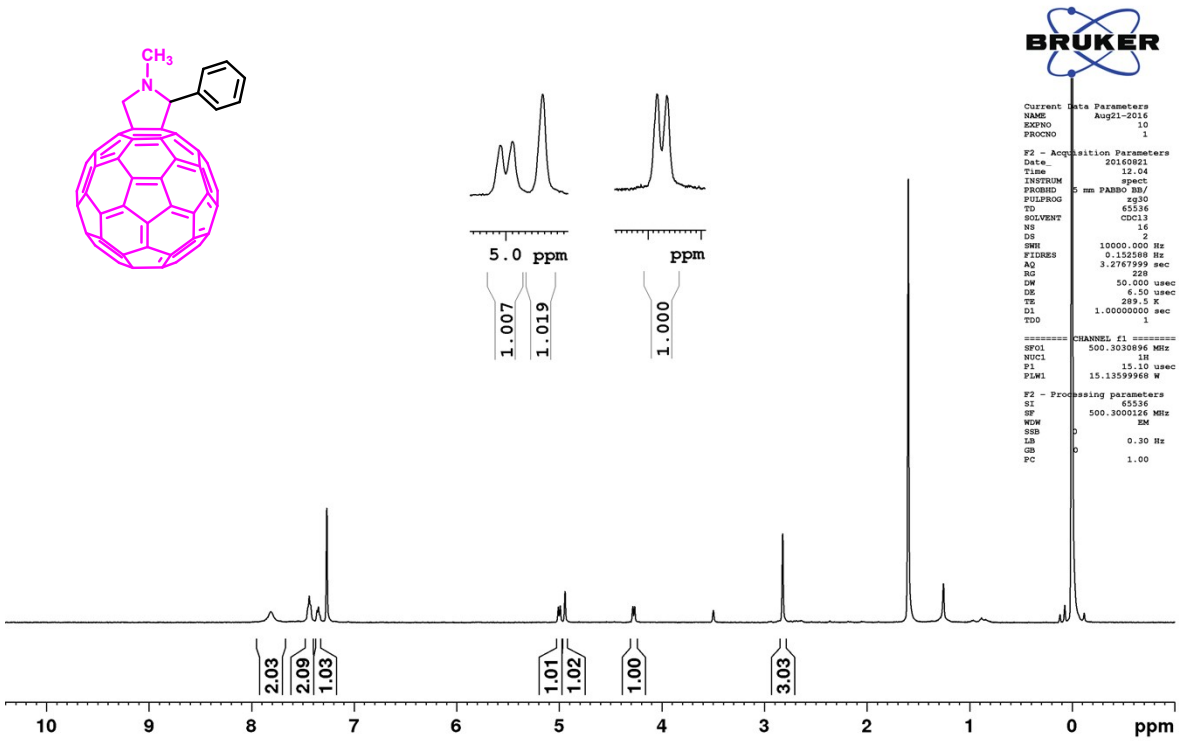

Fig. S9. ^{1}H NMR spectrum of *N*-Methyl-2-phenyl-3,4-fullero[60]pyrrolidine **(9)** in $CDCl_3$.

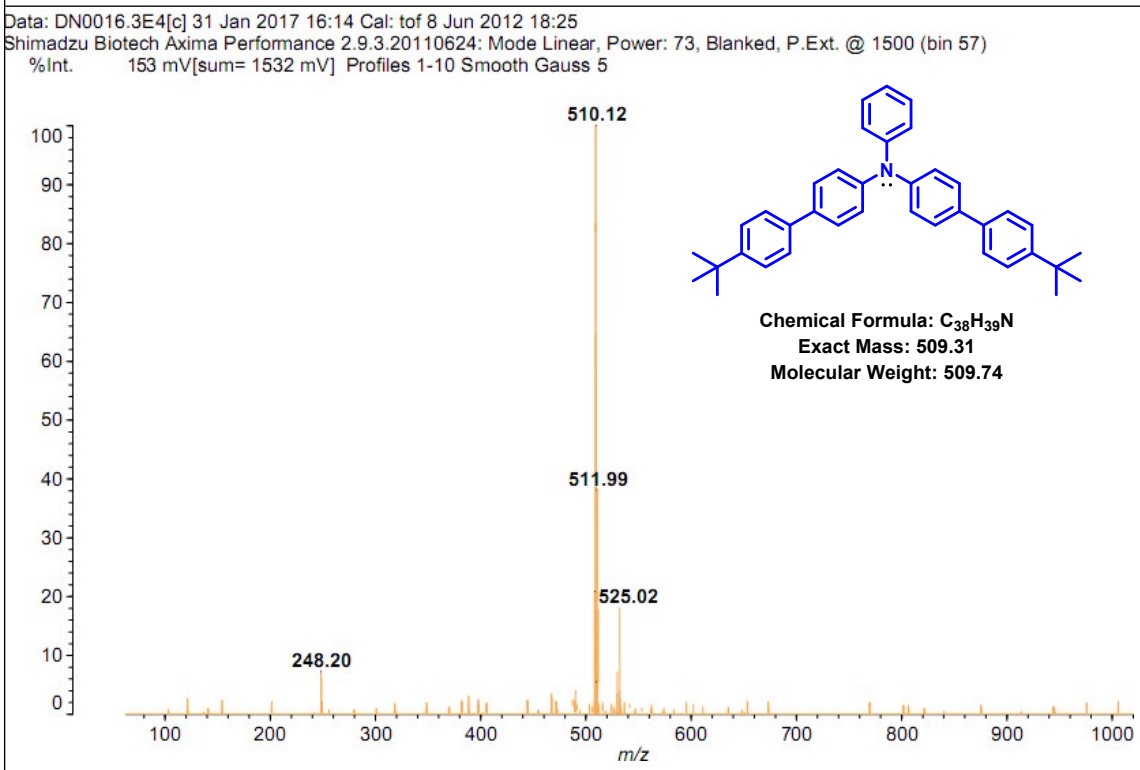

Fig. S10.MALDI-TOF spectrum of *N, N*-bis (4′-*tert*-butylbiphenyl-4-yl)aniline)**(1)**in $CDCl_3$.

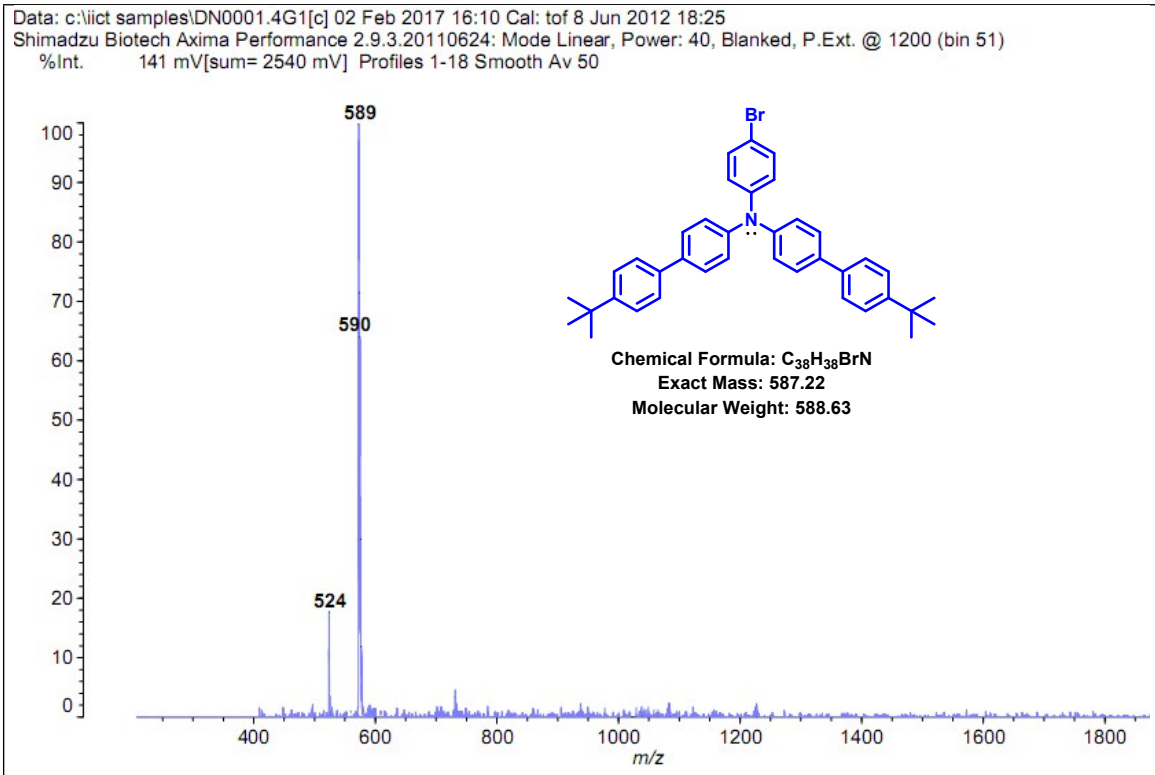

Fig. S11.MALDI-TOF spectrum of *N, N*-bis(4′-*tert*-butylbiphenyl-4-yl)4-bromoaniline **(2)**in $CDCl_3$.

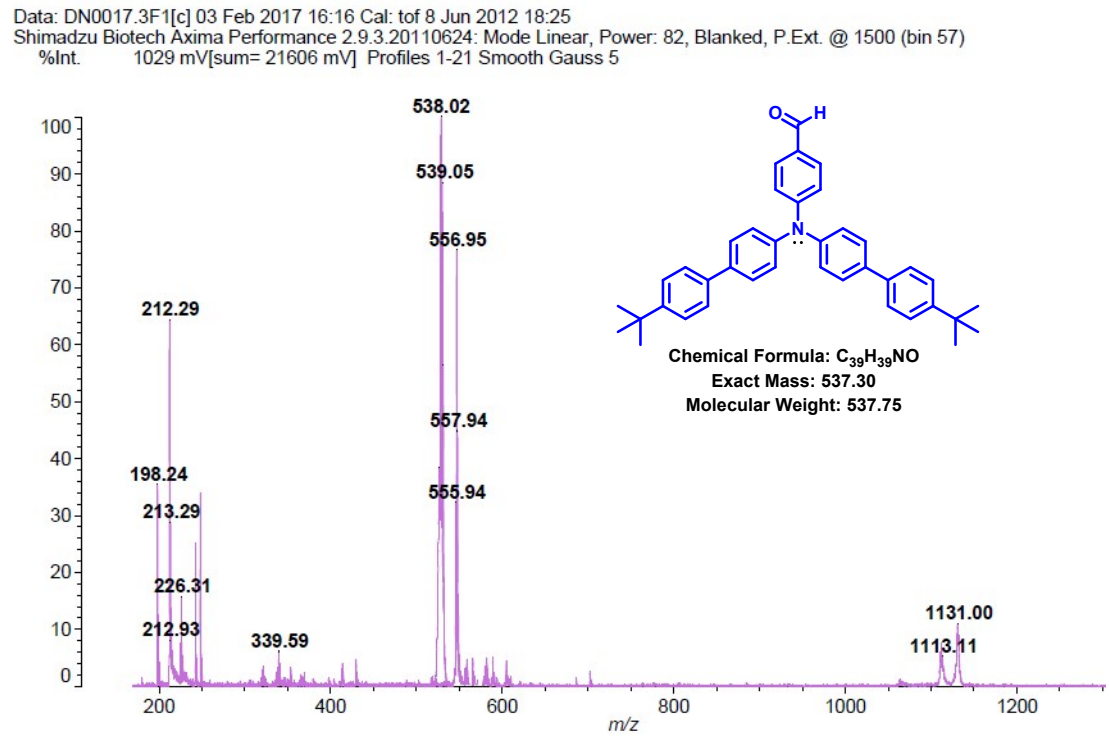

Fig. S12. MALDI-TOF spectrum of 4-(Bis(4′-*tert*-butylbiphenyl-4-yl)amino)benzaldehyde **(3)**in $CDCl_3$.

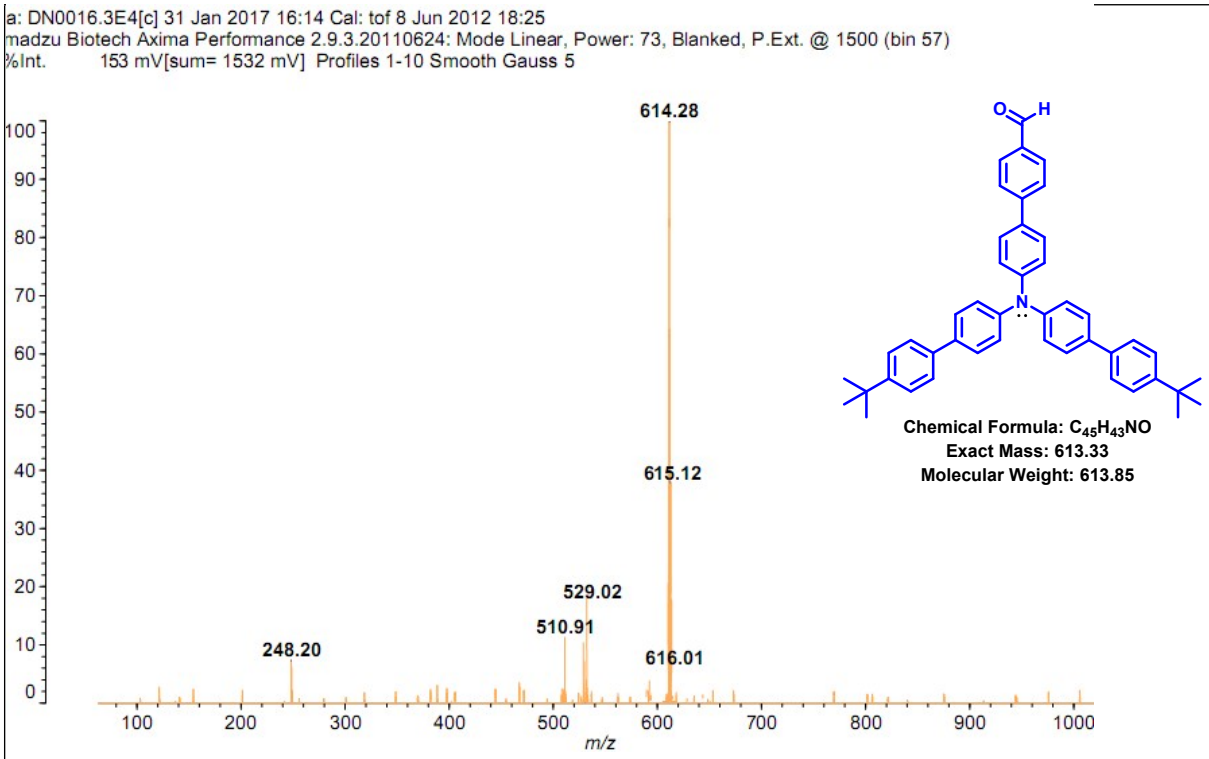

Fig. S13. MALDI-TOF spectrum of 4′-(Bis(4′-*tert*-butylbiphenyl-4-yl)amino)biphenyl-4-carbaldehyde **(4)**in $CDCl_3$.

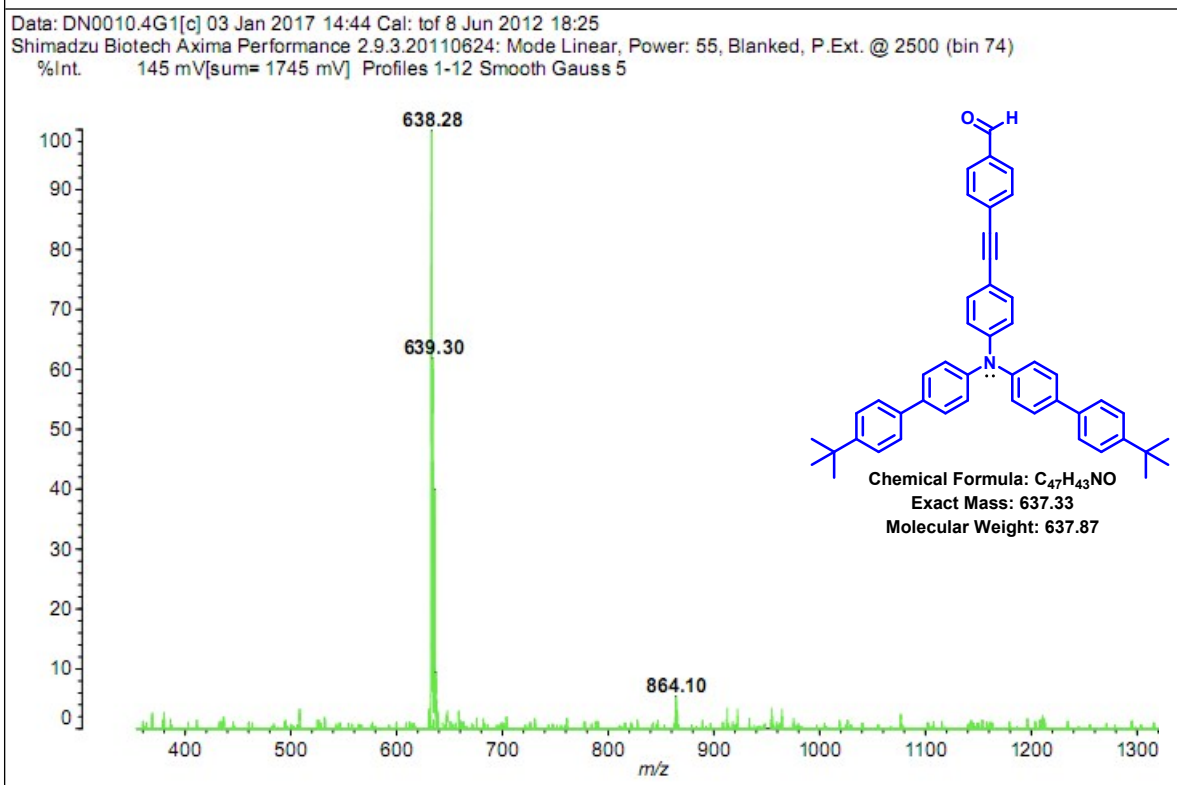

Fig. S14. MALDI-TOF spectrum of 4-(4-(Bis (4′-*tert*-butylbiphenyl-4-yl)amino)phenylethynyl)benzaldehyde **(5)** in $CDCl_3$.

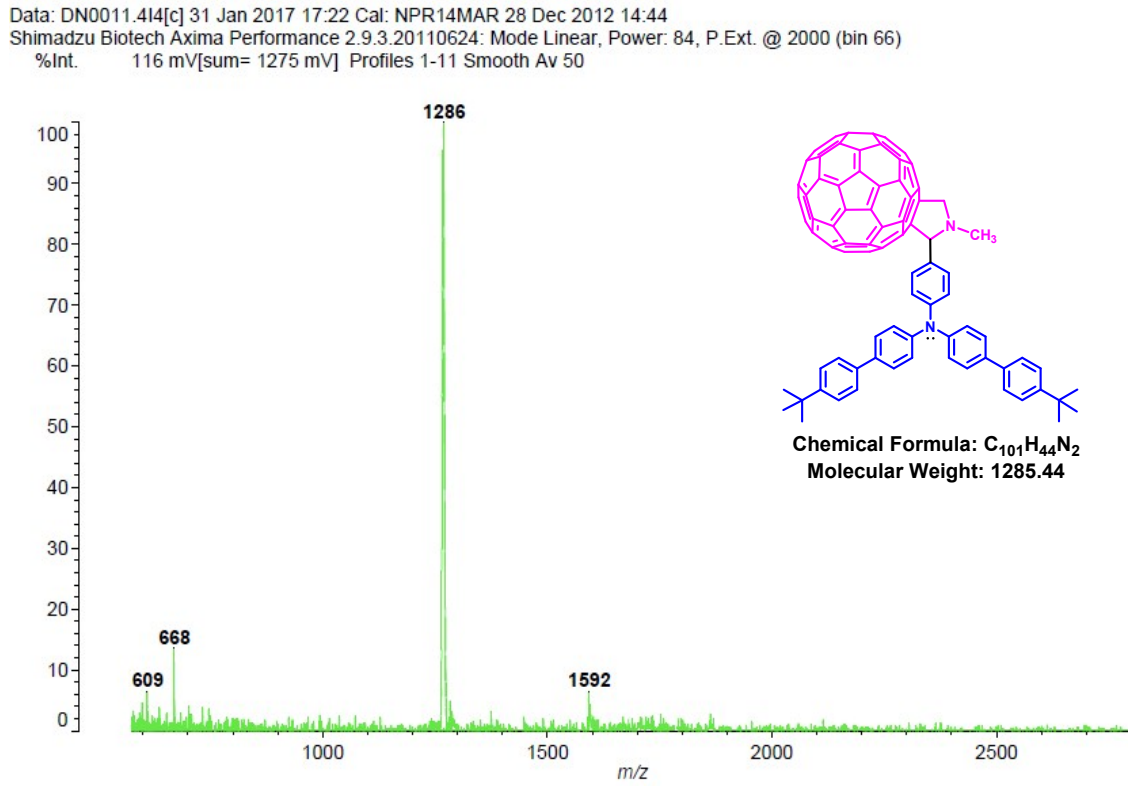

Fig. S15. MALDI-TOF spectrum of *N*-Methyl-2-(4-(bis(4′-tert-butylbiphenyl-4-yl)amino)phenyl)-3,4-fullero[60]pyrrolidine **(6)** in $CDCl_3$.

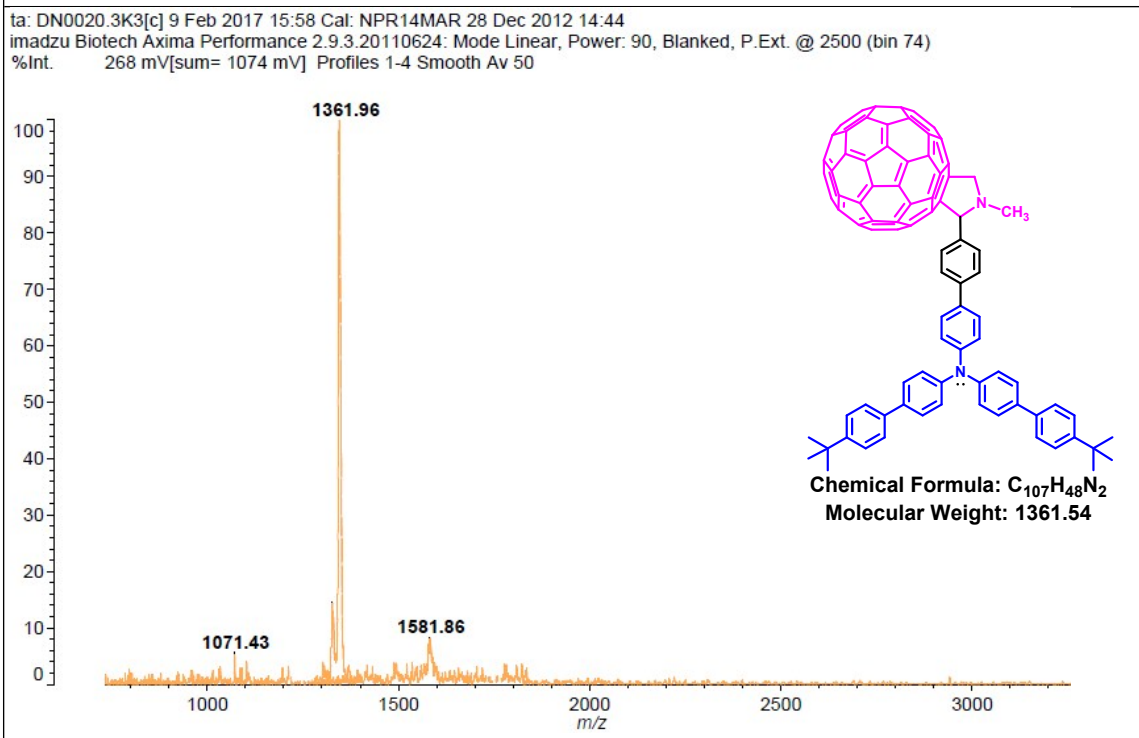

Fig. S16. MALDI-TOF spectrum of *N*-Methyl-2-(4′-(bis(4′-*tert*-butylbiphenyl-4-yl)amino)biphenyl-4-yl)-3,4-fullero[60]pyrrolidine **(7)** in $CDCl_3$.

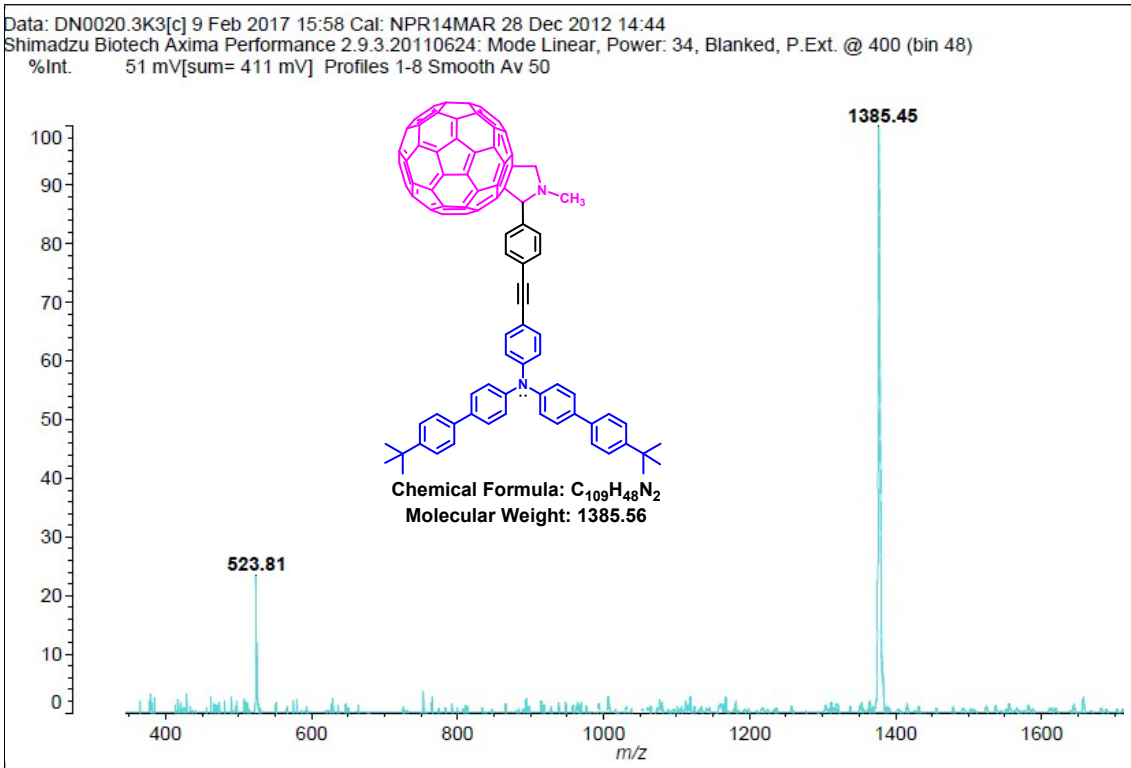

Fig. S17. MALDI-TOF spectrum of *N*-Methyl-2-(4-(4-(bis(4′-*tert*-butylbiphenyl-4-yl)amino)phenylethynyl)phenyl-3,4-fullero[60]pyrrolidine **(8)** in $CDCl_3$.

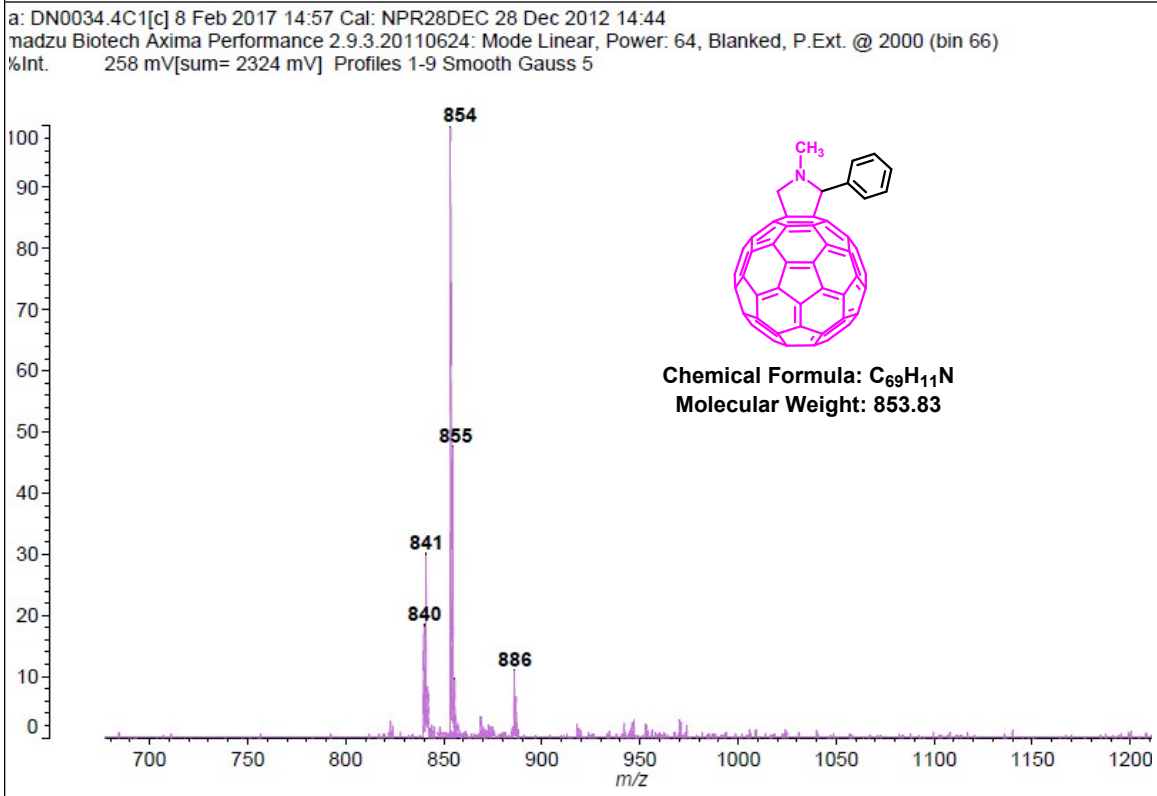

Fig. S18. MALDI-TOF spectrum of *N*-Methyl-2-phenyl-3,4-fullero[60]pyrrolidine**(9)**in $CDCl_3$.

TD-DFT Results

In order to gain a deeper understanding of the excited-state properties of the dyads, TD-DFT calculations using B3LYP energy functional with 6-31G(d,p) basis set with the framework of the polarizable continuum model (PCM) in toluene as solvent were performed and the results were found to be in reasonable agreement with the experimental values. The theoretical absorption spectra are shown in Figure S19 and related oscillation strength (f), excited state energy (E) in eV and the percentage contribution of molecular orbitals in the excited transitions are presented in Table S1

Dyad	HOMO	HOMO-1	LUMO	LUMO-1	R_{CC} Å	ΔE (eV)
Dyad-1	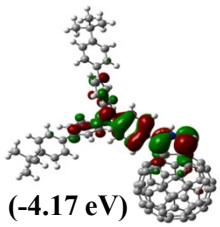 (-4.17 eV)	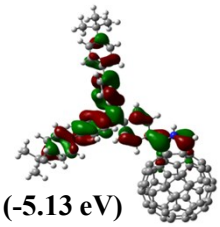 (-5.13 eV)	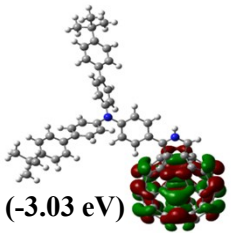 (-3.03 eV)	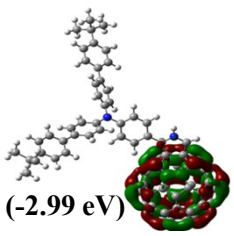 (-2.99 eV)	7.1	1.15
Dyad-2	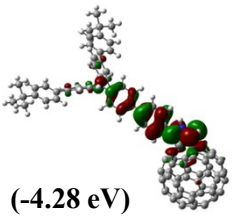 (-4.28 eV)	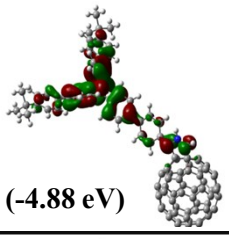 (-4.88 eV)	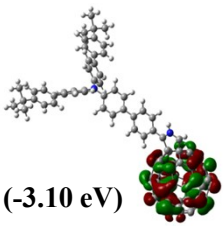 (-3.10 eV)	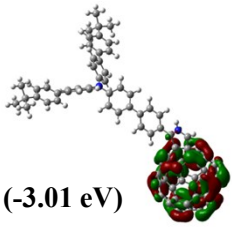 (-3.01 eV)	9.5	1.18
Dyad-3	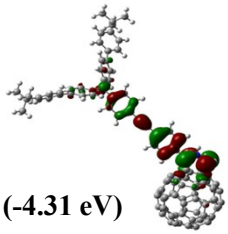 (-4.31 eV)	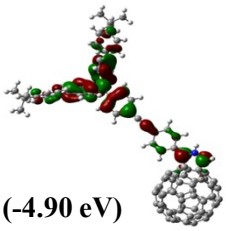 (-4.90 eV)	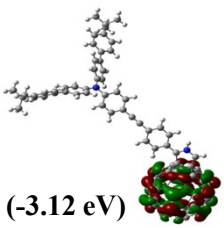 (-3.12 eV)	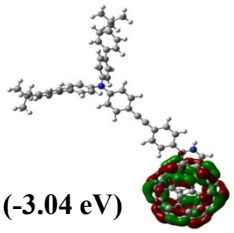 (-3.04 eV)	11.2	1.19

Fig. S19. Ground state optimized geometry and frontier molecular orbitals of the dyads. ΔE stands for HOMO-LUMO energy. Values in parenthesis are relative energy of the corresponding orbitals.

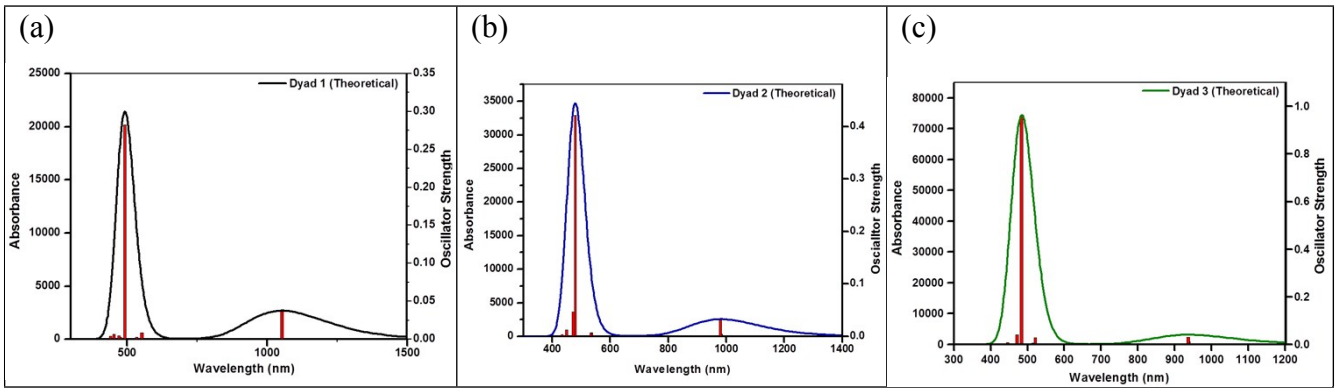

Fig. S20. Theoretical absorption spectra of (a) **Dyad-1**, (b) **Dyad -2**, and (c) **Dyad-3** calculated using B3LYP method PCM model in toluene solvent.

Table S1. Singlet excited state properties of by **Dyads 1-3** calculated by B3LYP method in toluene.

Dyads	[a]λ_{max}	[b]f	[c]E (eV)	% of Molecular Orbital Composition
Dyad 1	491	0.0005	1.16761	HOMO→LUMO (93%), HOMO→L+1 (3%)
		0.0365	1.17791	HOMO→L+1 (88%), H-1→L+1 (2%), HOMO→LUMO (3%), HOMO→L+4 (6%)
		0.0006	1.60901	HOMO→L+2 (92%), HOMO→L+6 (4%)
		0.0087	2.24172	HOMO→L+5 (89%), H-1→L+5 (4%)
		0.0027	2.32202	H-2→LUMO (93%), H-5→L+1 (2%)
Dyad 2	477	0.0043	1.26051	HOMO→LUMO (77%), HOMO→L+1 (18%)
		0.0308	1.26481	HOMO→LUMO (19%), HOMO→L+1 (72%), HOMO→L+4 (5%)
		0.0006	1.70181	HOMO→L+2 (92%), HOMO→L+6 (4%)
		0.0071	2.31812	H-2→LUMO (10%), HOMO→L+5 (79%), H-1→L+5 (2%)
		0.006	2.32632	H-2→LUMO (84%), HOMO→L+5 (9%)
Dyad 3	484	0.0124	1.32181	HOMO→LUMO (55%), HOMO→L+1 (38%), HOMO→L+4 (3%)
		0.0306	1.32351	HOMO→LUMO (41%), HOMO→L+1 (52%), HOMO→L+4 (3%)
		0.0007	1.76471	HOMO→L+2 (91%), H-1→L+2 (2%), HOMO→L+6 (2%)
		0.0023	2.32692	H-2→LUMO (93%)
		0.0289	2.37862	H-2→L+1 (18%), HOMO→L+5 (66%), H-5→LUMO (3%), H-3→LUMO (3%), H-1→L+5 (2%)

[a] theoretical absorbance in nm, [b]Oscillation strength, and [c]excited state energy in eV.

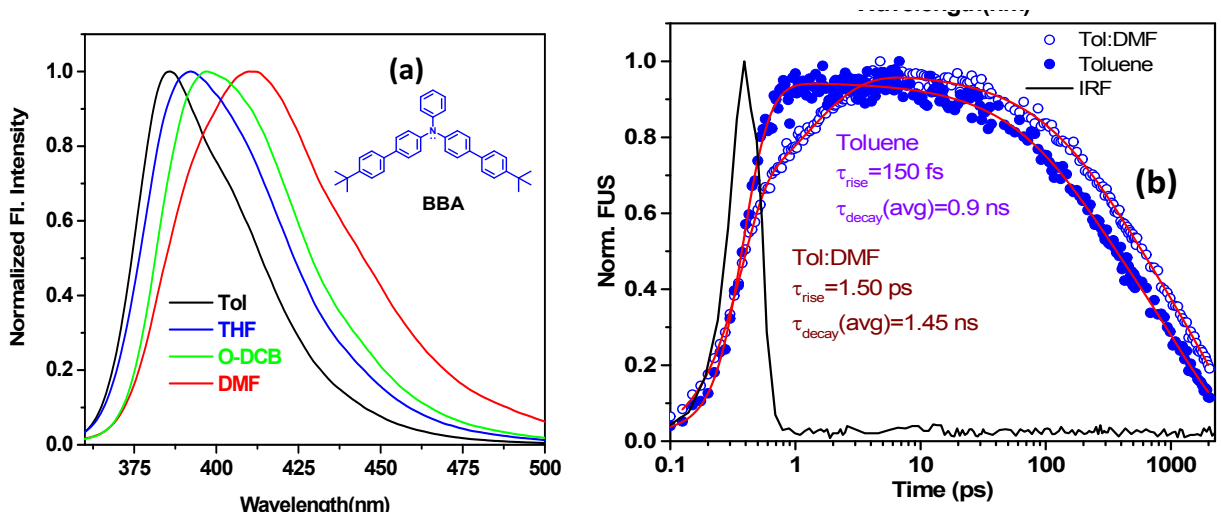

Fig. S21. Steady State Fluorescence emission spectra of isolated BBA in different solvents (a), fluorescence decay at 400 nm upon 370 nm excitation in toluene and Tol:DMF (b)

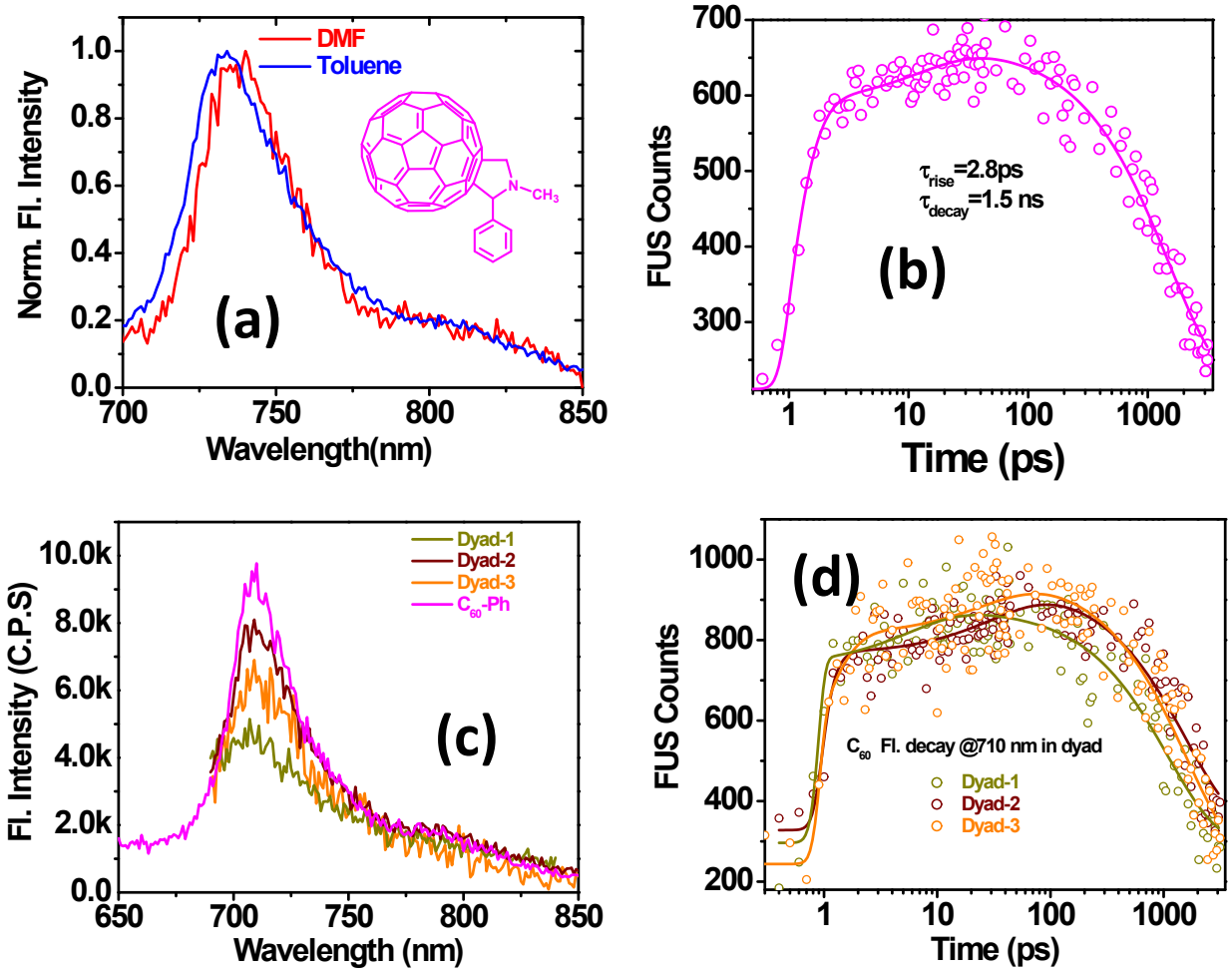

Fig. S22. Steady State Fluorescence emission spectra of isolated C_{60}-Ph in different solvents (a), fluorescence decay at 710 nm upon 370 nm excitation in Tol:DMF (b),Fluorescence of isolated C_{60}-Ph and C_{60} in dyad in Toluene and (d) Fluorescence decay of C_{60} in dyad in Toluene.

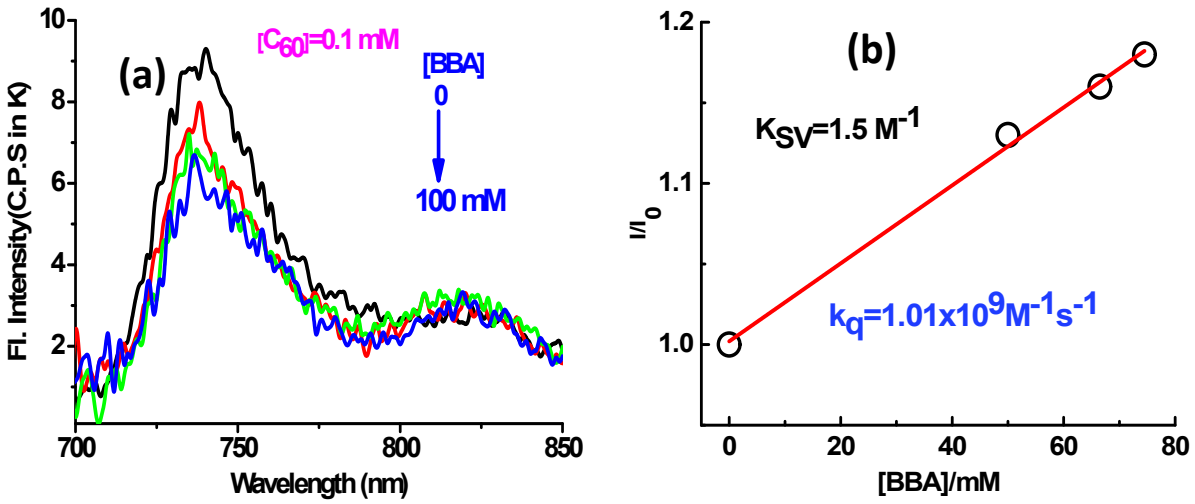

Fig. S23. Bimolecular fluorescence quenching of C_{60} in presence of BBA in 1:1(Tol:DMF) (a) and Linear S-V plot , I_o/I vs [BBA].

Table S2: Kinetic parameters of multi-exponential fits to TA time profiles at different wavelengths of isolated BBA in 1:1 (Tol-DMF), λ_{pump}=320nm

system	λ_{probe} (nm)	BBA Visible side τ_1,(a_1%)/fs	τ_2,(a_2%)/ps	τ_3,(a_3%)/ns	λ_{probe} (nm)	BBA IR side τ_1,(a_1%)/ps	τ_2,(a_2%)/ps	τ_3,(a_3%)/ns
Isolated BBA	485	250(-25)	100 (10)	1.8(100)	870	4.5(-30)	456(50)	2.6(50) 1.5*(100)
	550	700(-15)	1000(-30)	2(100)	970	1.7(-50)	440 (50)	2.3(50) 1.4*(100)
	635	---	2000(-37)	3(100)				

*Weighted average value of τ_2 &τ_3

Table S3: Kinetic parameters of multi-exponential fits to TA time profiles at different wavelengths of isolated C_{60}-Ph in Toluene and 1:1 (Tol-DMF), λ_{pump}=485 nm

Solvent	λ_{probe} (nm)	C_{60} Visible side τ_1,(a_1%)/fs	τ_2,(a_2%)/ns	τ_3,(a_3%)/μs	λ_{probe} (nm)	C_{60} IR side τ_1,(a_1%)/ps	τ_2,(a_2%)/ps	τ_3,(a_3%)/ns
Tol:DMF	700	25 (-15)	2.1(-50)	1 (100)	900	29 (5)	1030(65)	8.5(30)
	750	25 (-17)	0.59(-17)	0.1(100)	1020	30(-20)	615 (32)	2.0(68)1.56*(100)
Tol	700	31(-20)	1.7(-50)	1.6 (100)	900	36 (5)	1200 (62)	8 (33)
	750	30 (-18)	1 (-50)	1(100)	1020	26 (-17)	----	1.5 (100)

Table S4: Kinetic parameters of dyads in toluene solution upon 320 and 485 nm excitation at different selected wavelengths of TA absorption spectra.

system	Pump (nm)	Visible region					IR region				
		λ_{prob} (nm)	τ_1, (a_1%)/ps	τ_2,(a_2%) /ps	τ_3,(a_3%) /ns	τ_4,(a_4%)/µs	λ_{probe} (nm)	τ_1, (a_1%)/ps	τ_2,(a_2%)/ps	τ_3,(a_3%) /ns	τ_4,(a_3%) /µs*
Dyad-1	320	530	0.24(57)	30 (2)	1.4(15)	1.5 (26)	900	0.3(15)	30 (-23)	1.6(70)	≡1.5(15)
		700	0.23(13)	25(-10)	3.4(-40)	0.15(87)	1020	-----	31(-24)	1.6(81)	≡1.5(19)
	433	530		---	1.1(-45)	0.15(100)	900	------	35(-31)	1.5(81)	≡1.5(19)
		700	-----	27(-33)	3.2(-13)	1.5(100)	1020	------	35(-28)	1.7(89)	≡1.5(11)
Dyad-2	320	530	0.3(68)	22(4)	1.3(11)	1.5(18)	900	0.6(23)	28(2)	1.3(60)	≡1.5(15)
		700	0.34(30)	39(4)	1.3(-20)	1.5(70)	1020	0.5(35)	32(-10)	1.4(55)	≡1.5(10)
	485	530	-----	2(15)	1.1(-15)	1.5(85)	900	----	23 (4)	1.4(81)	≡1.5(15)
		700	------	23(-4)	2.1(-46)	1.5(100)	1020	----	23(-80)	1.6(42)	≡1.5(58)
Dyad- 3	320	530	0.4(76)	30(2)	1.5 (9)	1.5(13)	900	0.9(25)	5.1(6)	1.4(55)	≡1.5(14)
		700	0.4(80)	30(1)	1.3(10)	1.5(9)	1020	1.3(30)	42(-6)	1.5(60)	≡1.5(10)
	485	530	-----	30(-2)	2.2(-28)	1.5(100)	900	-------	19(-9)	1.45(54)	≡1.5(31)
		700	-----	-----	1.5(45)	1.5(50)	1020	-------	24(-15)	1.6 (62)	≡1.5(21)

* constrain of the fit

TA of C_{60}-Ph in toluene and 1:1 Tol:DMF

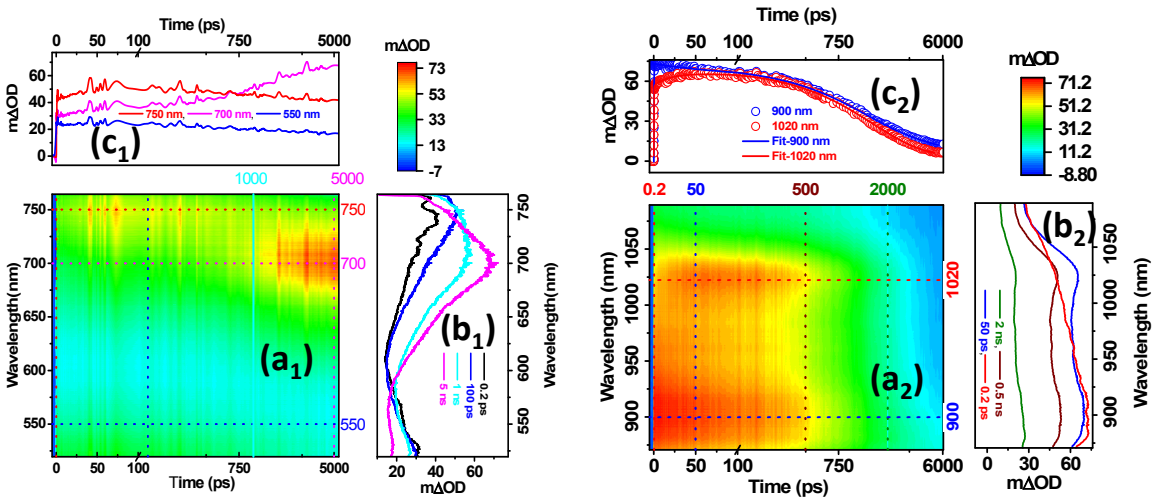

Fig. S24. Overview of TA data matrices in range of detection wavelength (visible and IR regions) of **C_{60}-Ph** upon 485 nm excitation (pumping) in toluene solution. (a_1, a_2) are ΔOD heat maps, (b_1, b_2) are evolution of TA spectra a different times and (c_1, c_2) are time profiles at specific wavelengths in Vis and IR region respectively in toluene solution.. Note that time axis is linear until 3 ps and logarithmic thereafter.

Supporting Information

Figure S24(a-f) is the profile picture TA data of isolated C_{60}-Ph in 1:1(Tol:DMF) solution which pictorially summarizes the gross transient behaviour of C_{60} relaxation processes (see Figure S23 in toluene). Immediately after excitation, it shows very strong and broad ESA (hot $S_1 \rightarrow S_n$) all over the detected wevelength region (500-1100 nm) and it relaxed within couple of ps time scale to a more structure ESA spectra ($S_1 \rightarrow S_n$) with a characteristic peak at 1020 nm. Finally, in few nanosecond time scale it evolves to a new and relatively narrow ESA spectra ($T_1 \rightarrow T_n$) peaking at 700nm (see Figure S23 in Toluene solution). The global and target analysis of TA data is successfully performed with three compartmental model corresponding to hot S_1, thermally relaxed S_1 and lowest triplet T_1 accommodating internal conversion and/or vibrational relaxation (IC/VR) from hot S_1 to S_0 with rate constant k_1, very less contribution of radiative decay from S_1 to S_0 (k_2) and predominant nonradiative transition leading to intersystem crossing (ISC)(S_1 to T_1 (k_3)) and finally deactivation of T_1 to S_0 by k_4 (Figure 6g). The estimated population time profiles and corresponding SADS resulting from global and target analysis of the data matrix obtained in 1:1 (Tol: DMF) solution are shown in Figure 6h and Figure 6i respectively. The $SADS_1$ represents the hot S_1 state with estimated global lifetime of 25 ps and $SADS_2$ corresponds thermally stable S_1 state with 1.3 ns lifetime and this lifetime values nicely corroborates to the value of $^1C_{60}^*$ lifetime measured from fluorescence decay. However, the most interesting feature of the $SADS_2$ is the appearance of narrow and sharp absorption peak at 1020 nm and to the best of our knowledge this is the first report to its kind so far. The $SADS_3$ signifies to T_1 state with a lifetime value of ~0.2 μs, although determination of lifetime value in 6 ns time domain data is hardly possible.

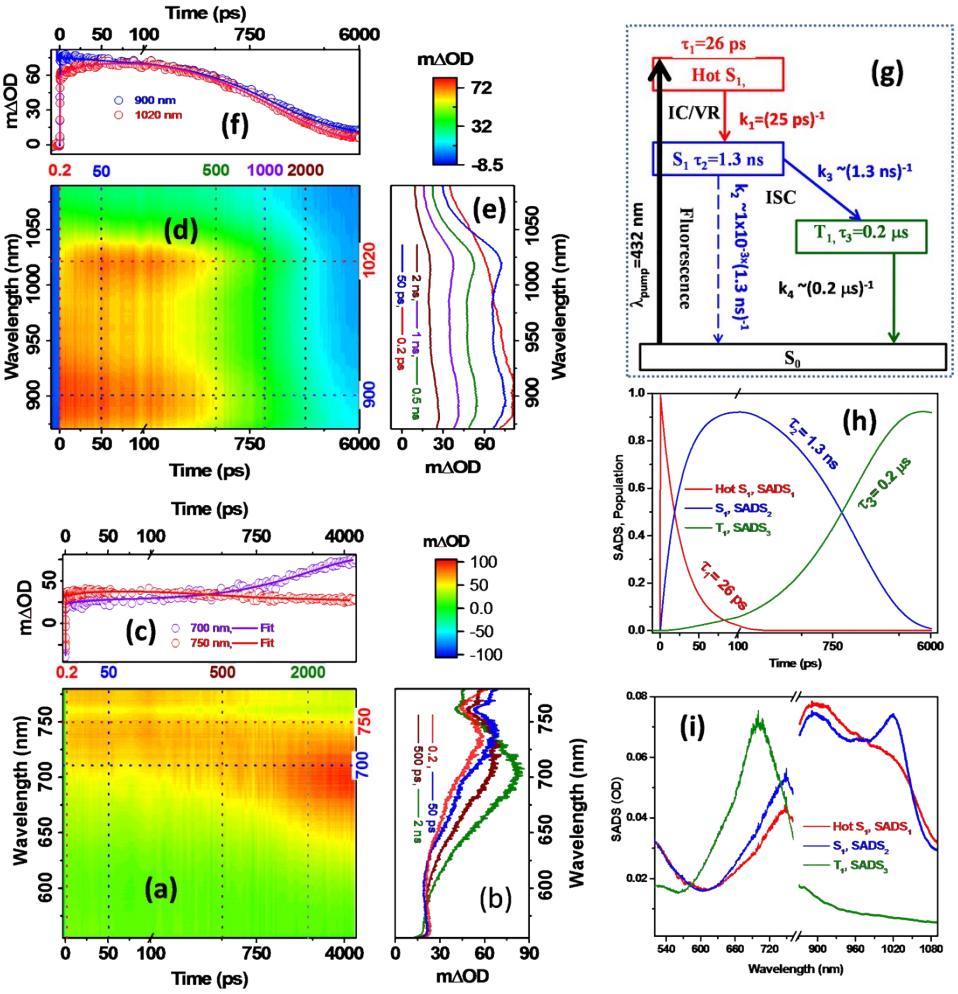

Fig. S25. Profile picture of transient absorption data of C_{60}-Ph (0.2 mM) in 1:1(Tol:DMF) upon 485 nm excitation. ΔOD heat map as a function of probe wavelength (vertical) and probe delay (horizontal) of C_{60} in Vis region (a) and in IR region (d). As indicated in the color map, the zero level is colored in light-green, green to red indicates positive signals (i.e., photoinduced absorption), and blue denote negative signals (i.e., decrease in absorption due to stimulated emission and/or ground-state bleaching if any). TA spectra at selected delay times (b, d) and time traces at selected probe wavelengths (e, f) for respective spectral windows. Vertical dotted lines in heat map indicate the position of selected delay times whereas horizontal dotted lines indicate position of selected wavelengths for which TA spectra and time profiles are plotted in (b,e) and (c,f) respectively. Kinetic scheme used for target analysis of the TA data (g). Estimated rate constant and global lifetimes are given in the scheme. (h,i) The population profiles and respective SADSs. Note that for better visualization the time axis of heat map is kept linear until 100 ps and logarithmic thereafter, similarly, in population profile X-axis is linear till 100 ps and logarithmic thereafter.

TA of all three Dyads in toluene

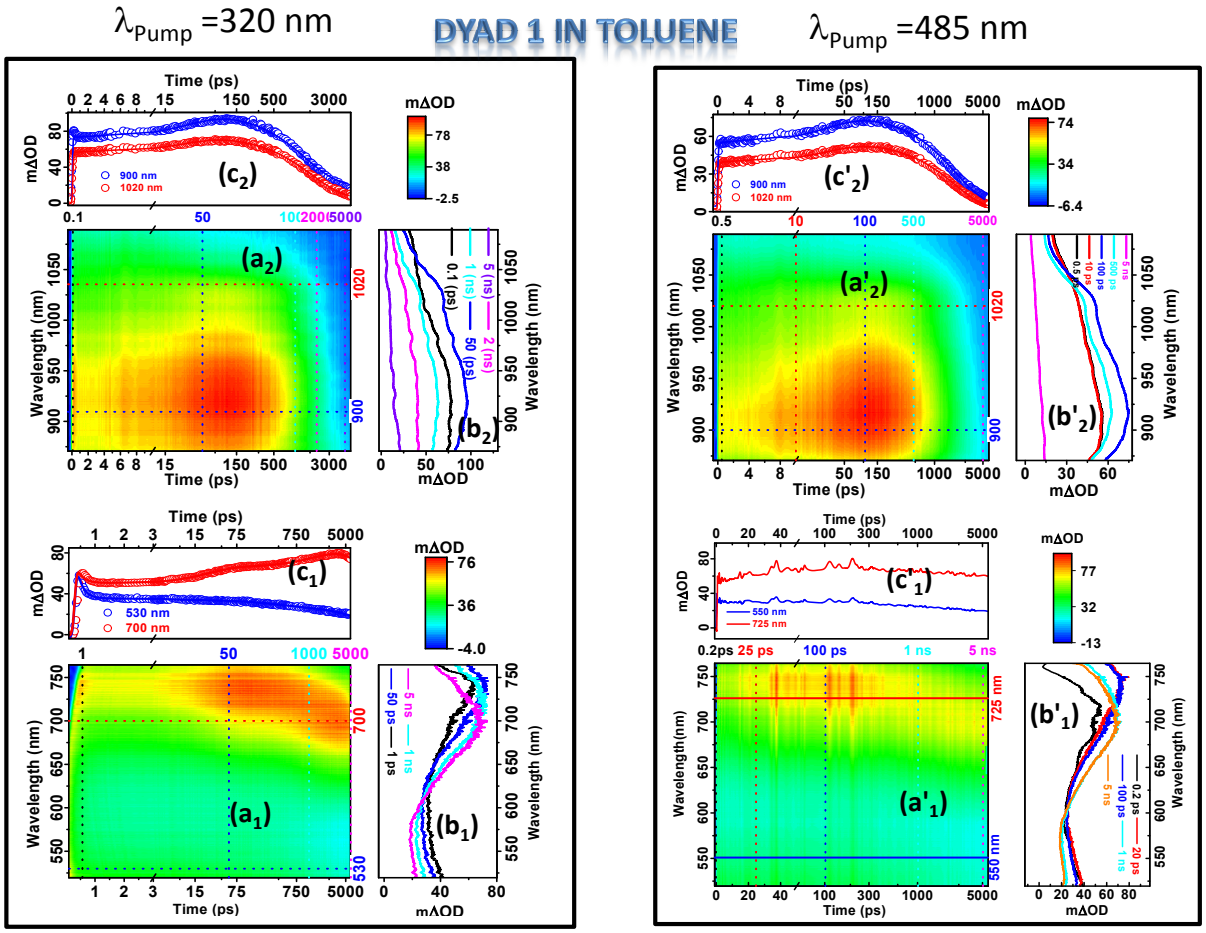

Fig. S26. Comparative overview of TA data matrices in the range of detection wavelength (visible and IR regions) of **Dyad-1** upon 320 and 485 nm excitation (pumping) in toluene solution. (a_1, a_2) are ΔOD heat maps (b_1, b_2) are evolution of TA spectra at different delay times and (c_1, c_2) are time profiles at specific wavelengths in Vis and IR region respectively when λ_{pump}=320 nm. Similarly, (a'_1, a'_2) are ΔOD heat maps (b'_1, b'_2) are evolution of TA spectra at different delay times and (c'_1, c'_2) are time profiles at specific wavelengths in Vis and IR region respectively when λ_{pump}=485 nm. Note that time axis is linear until slash (/) mark shown, and logarithmic thereafter.

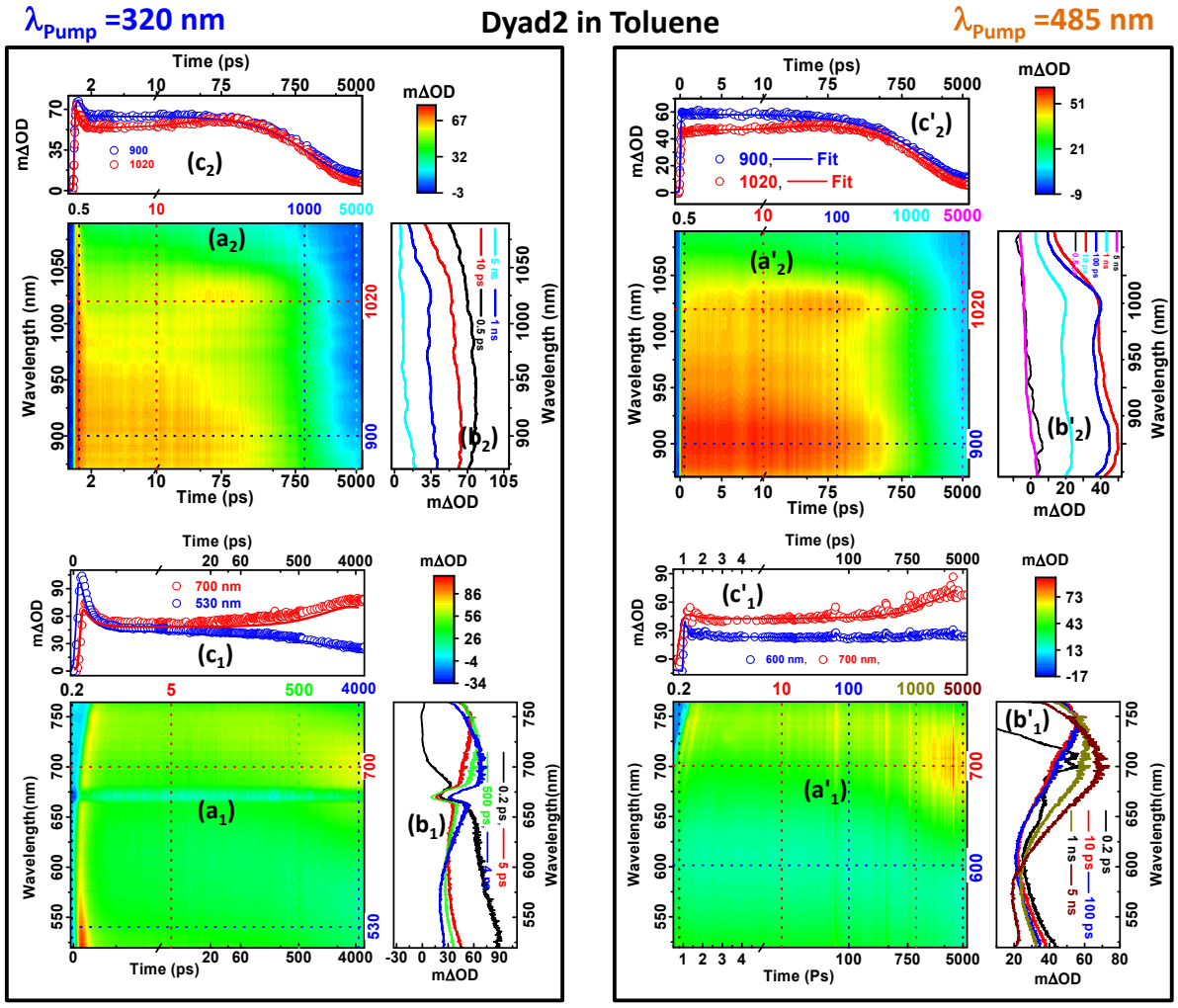

Fig. S27.Comparative overview of TA data matrices in the range of detection wavelength (visible and IR regions) of **Dyad-2** upon 320 and 485 nm excitation (pumping) in toluene solution. (a_1, a_2) are ΔOD heat maps (b_1, b_2) are evolution of TA spectra at different delay times and (c_1, c_2) are time profiles at specific wavelengths in Vis and IR region respectively when λ_{pump}=320 nm. Similarly, (a'_1, a'_2) are ΔOD heat maps (b'_1, b'_2) are evolution of TA spectra at different delay times and (c'_1, c'_2) are time profiles at specific wavelengths in Vis and IR region respectively when λ_{pump}=485 nm. Note that time axis is linear until slash (/) mark shown, and logarithmic thereafter

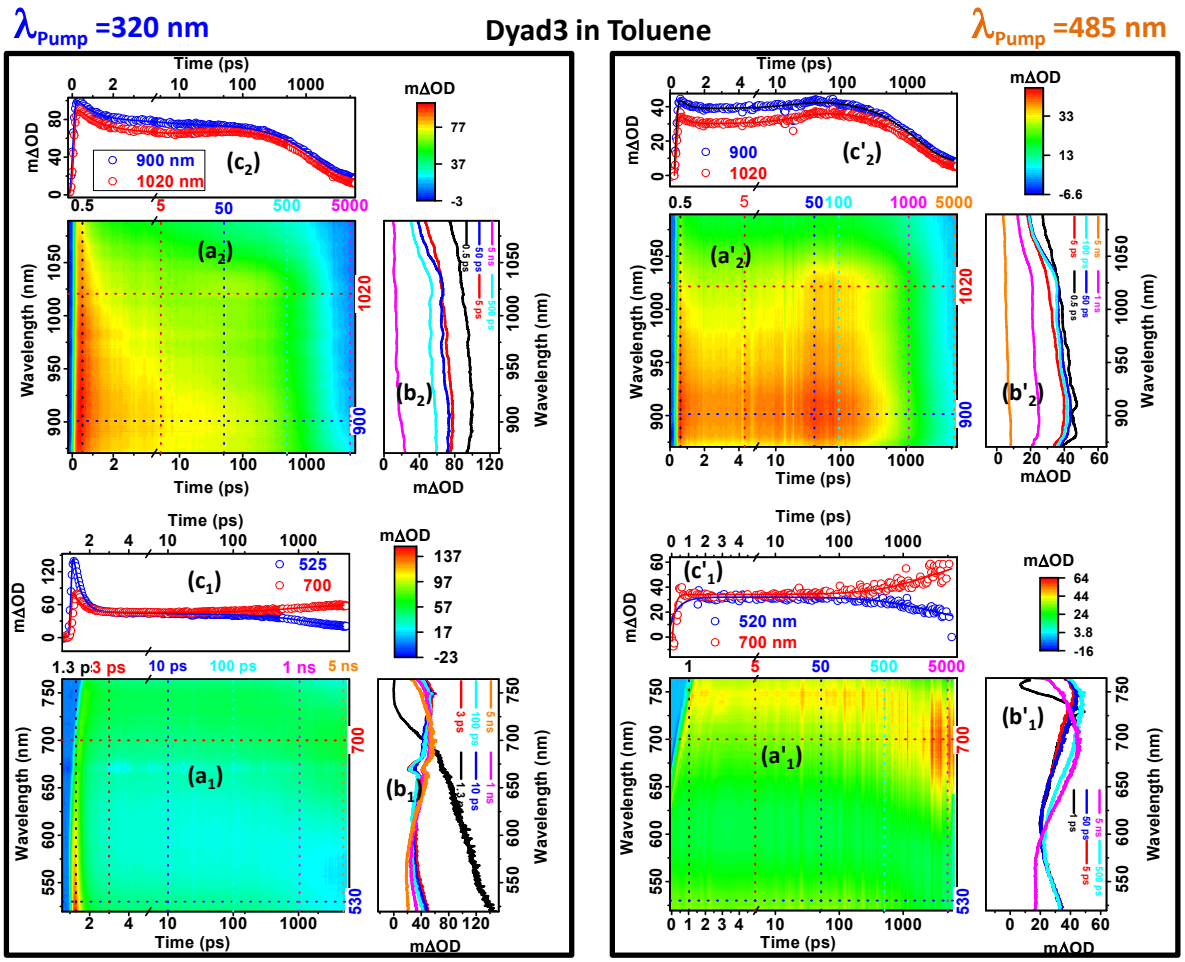

Fig. S28. Comparative overview of TA data matrices in the range of detection wavelength (visible and IR regions) of **Dyad-3** upon 320 and 485 nm excitation (pumping) in toluene solution. (a_1, a_2) are ΔOD heat maps (b_1, b_2) are evolution of TA spectra at different delay times and (c_1, c_2) are time profiles at specific wavelengths in Vis and IR region respectively when λ_{pump}=320 nm. Similarly, (a'_1, a'_2) are ΔOD heat maps (b'_1, b'_2) are evolution of TA spectra at different delay times and (c'_1, c'_2) are time profiles at specific wavelengths in Vis and IR region respectively when λ_{pump}=485 nm. Note that time axis is linear until slash (/) mark shown, and logarithmic thereafter

TA of Dyad-1 and Dyad-3 and 1:1 Tol:DMF

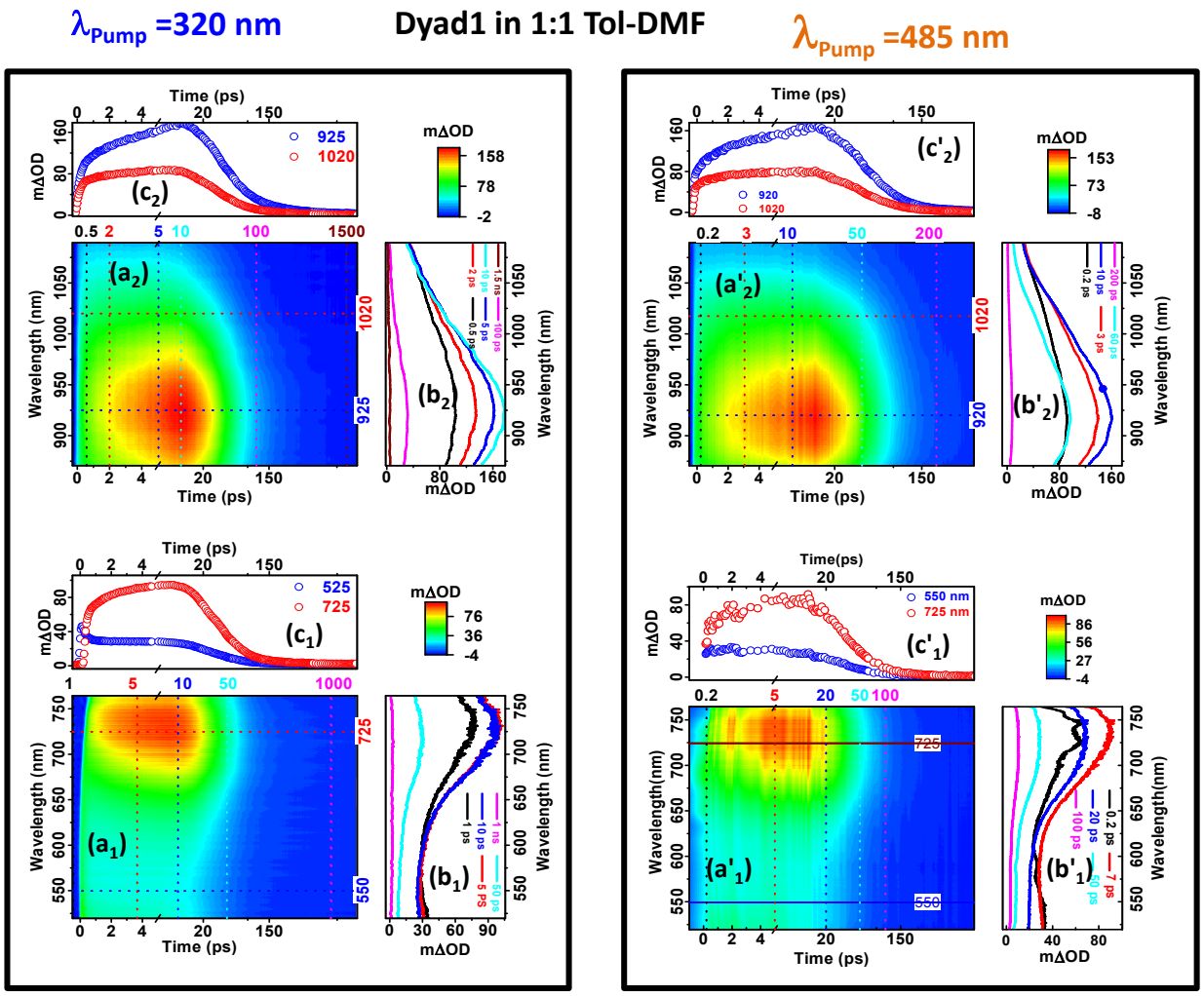

Fig. S29. Comparative overview of TA data matrices in the range of detection wavelength (visible and IR regions) of **Dyad-1** upon 320 and 485 nm excitation (pumping) in 1:1 Tol-DMF solution. (a_1, a_2) are ΔOD heat maps (b_1, b_2) are evolution of TA spectra at different delay times and (c_1, c_2) are time profiles at specific wavelengths in Vis and IR region respectively when λ_{pump}=320 nm. Similarly, (a'_1, a'_2) are ΔOD heat maps (b'_1, b'_2) are evolution of TA spectra at different delay times and (c'_1, c'_2) are time profiles at specific wavelengths in Vis and IR region respectively when λ_{pump}=485 nm. Note that time axis is linear until slash (/) mark shown and logarithmic thereafter

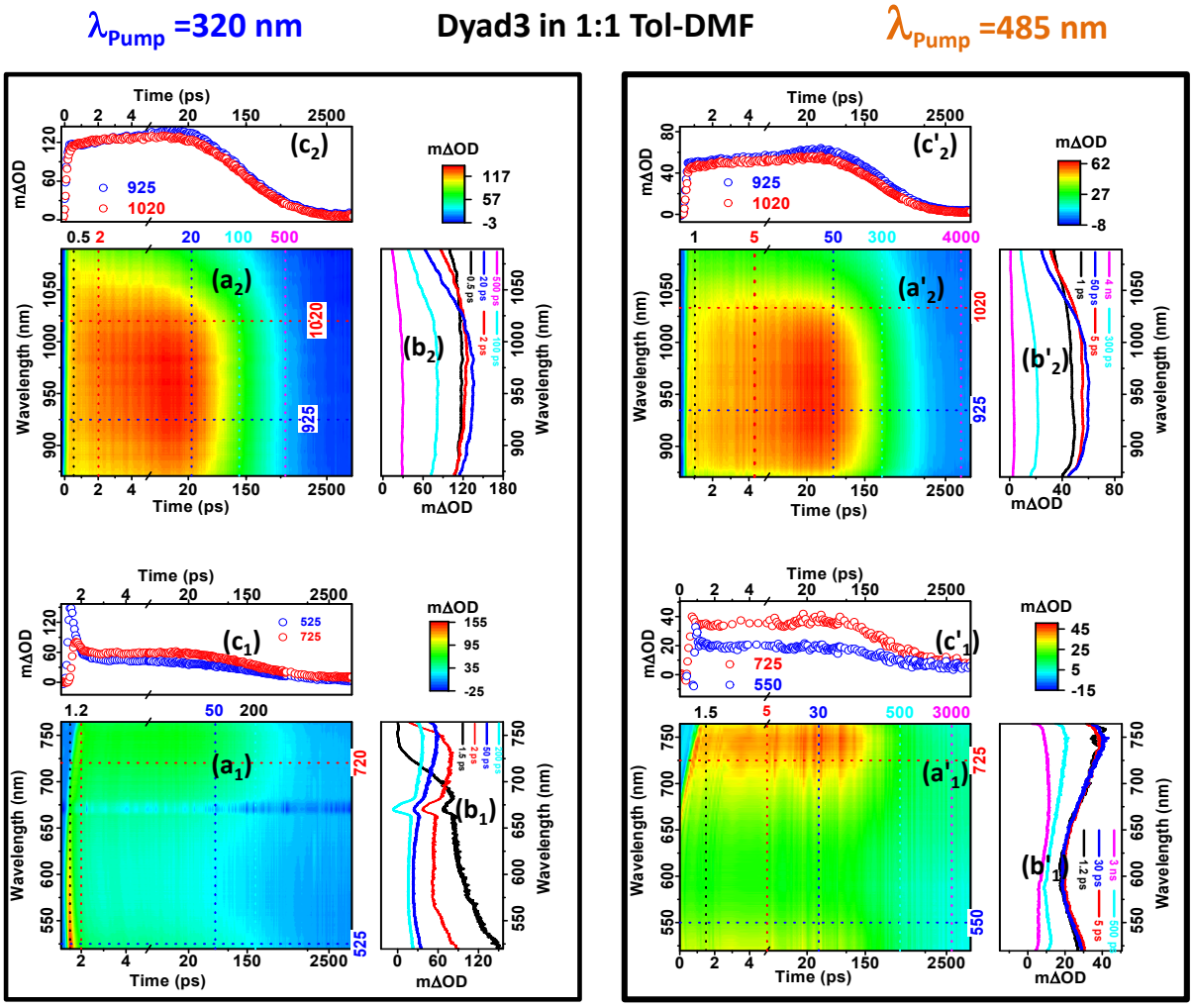

Fig. S30. Comparative overview of TA data matrices in the range of detection wavelength (visible and IR regions) of **Dyad-3** upon 320 and 485 nm excitation (pumping) in 1:1 Tol-DMF solution. (a_1, a_2) are ΔOD heat maps (b_1, b_2) are evolution of TA spectra at different delay times and (c_1, c_2) are time profiles at specific wavelengths in Vis and IR region respectively when λ_{pump}=320 nm. Similarly, (a'_1, a'_2) are ΔOD heat maps (b'_1, b'_2) are evolution of TA spectra at different delay times and (c'_1, c'_2) are time profiles at specific wavelengths in Vis and IR region respectively whenλ_{pump}=485 nm. Note that time axis is linear until slash (/) mark shown and logarithmic thereafter

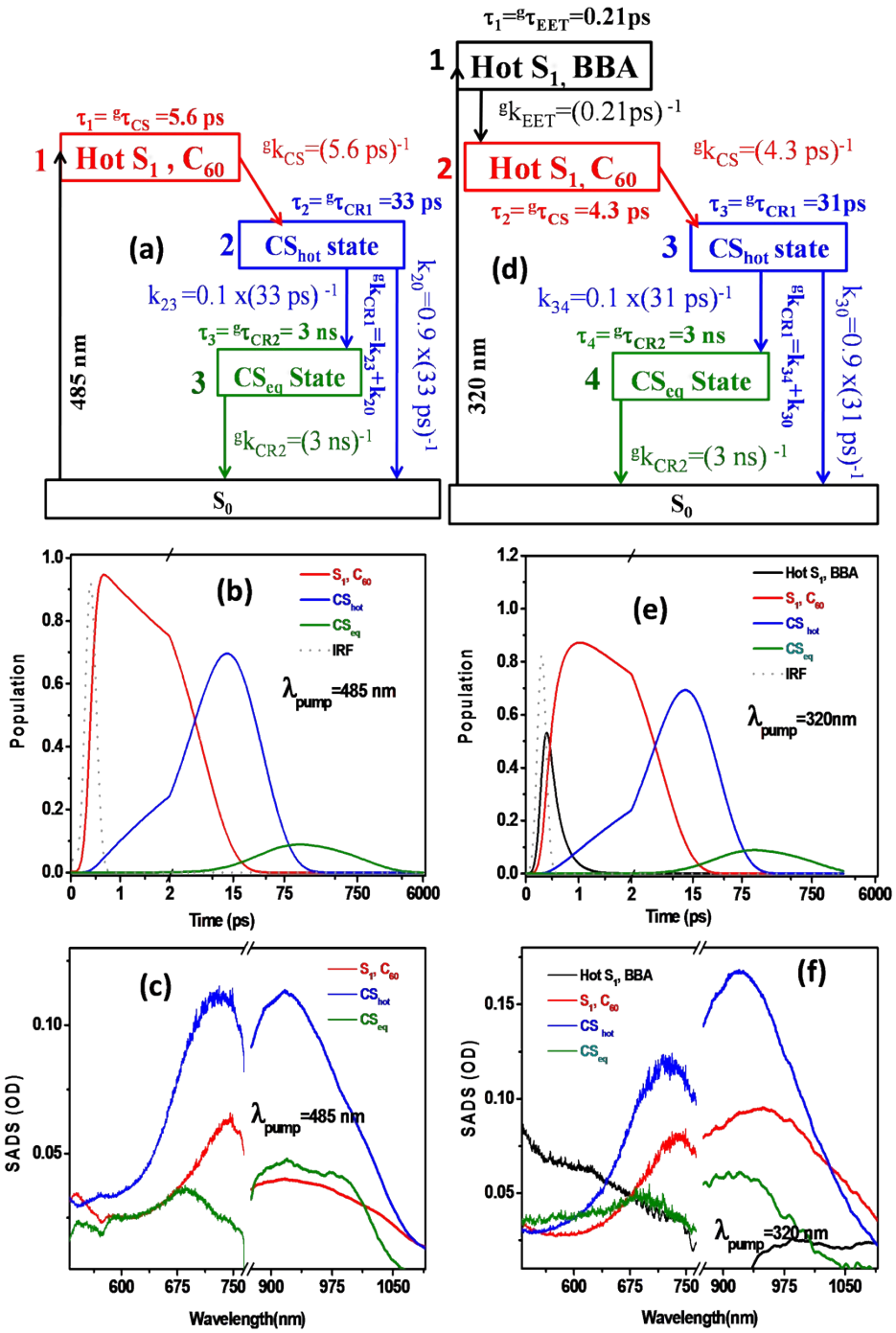

Fig. S31. (a,d) Kinetic scheme used for global and target analysis of the 485 and 320 nm excitation data respectively for **Dyad-1** in 1:1 (Tol:DMF) solution. The estimated rate constants are indicated in the figure: (a) the global lifetimes are 5.6 ps (hot S_1, C_{60}), 33 ps (CS_{hot} state) and 3 ns (CS_{eq}) when excitation is 485nm ,(d) the global lifetimes are 0.21 ps (hot S_1, BBA), 4.3ps (hot S_1, C_{60}) 31 ps (CS_{hot} state) and 3 ns (CS_{eq}) when excited at 320 nm (b,e) The population profiles and (c,f) estimated SADS upon 485 and 320 nm excitation respectively. The time axis is linear until 2 ps and logarithmic thereafter.

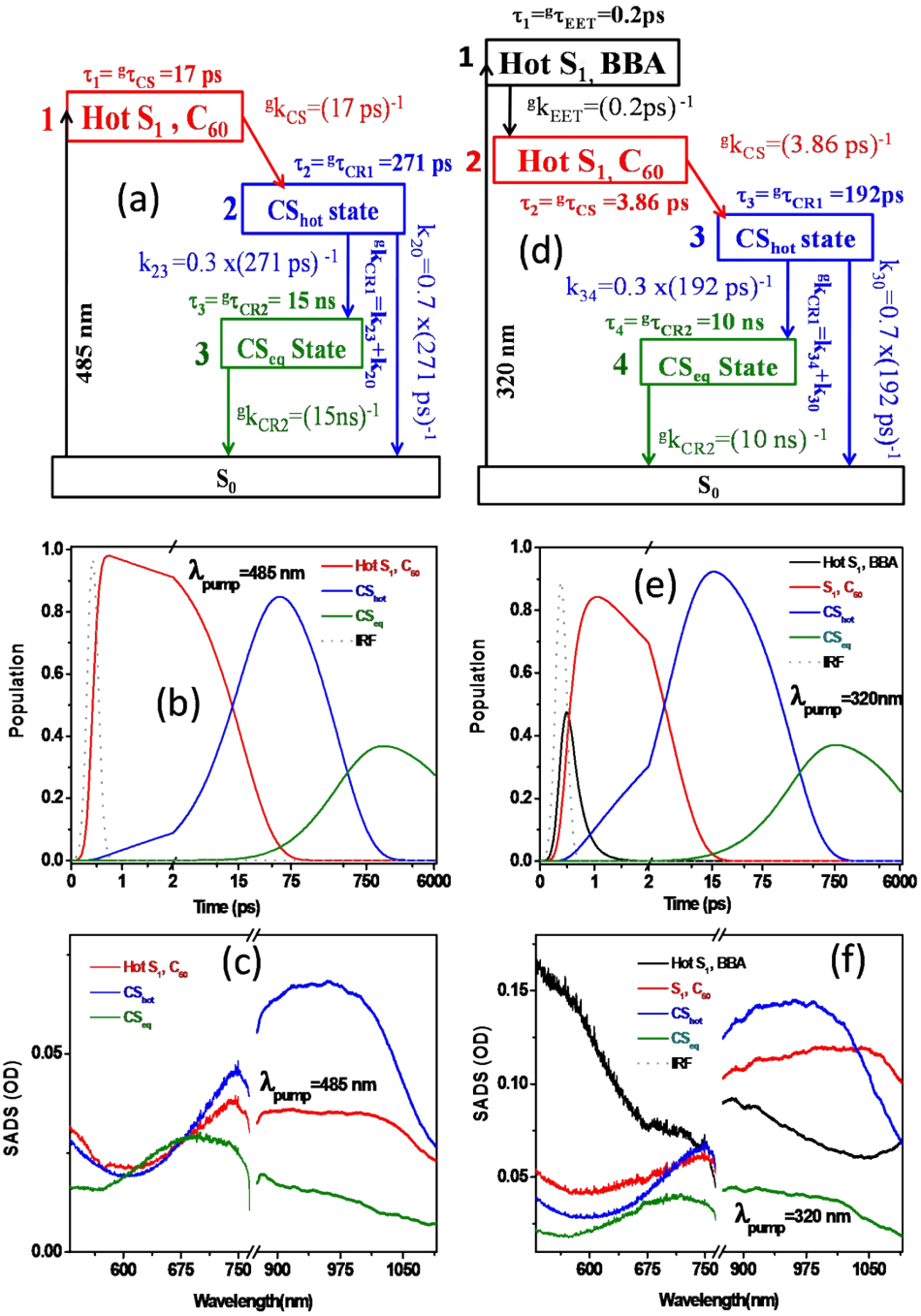

Fig. S32.-(a,d) Kinetic scheme used for global and target analysis of the 485 and 320 nm excitation data respectively for **Dyad-3** in 1:1 (Tol:DMF) solution. The estimated rate constants are indicated in the figure: (a) the global lifetimes are 17ps (hot S_1, C_{60}), 271ps (CS_{hot} state) and 15 ns (CS_{eq}) when excitation is 485nm ,(d) the global lifetimes are 0.2 ps (hot S_1, BBA), 3.86ps (hot S_1, C_{60}) 192ps (CS_{hot} state) and 10 ns (CS_{eq}) when excited at 320 nm (b,e) The population profiles and (c,f) estimated SADS upon 485 and 320 nm excitation respectively. The time axis is linear until 2 ps and logarithmic thereafter.

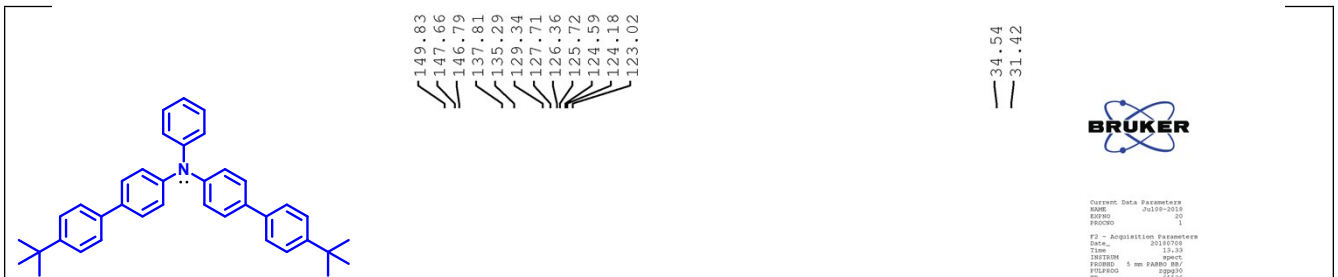

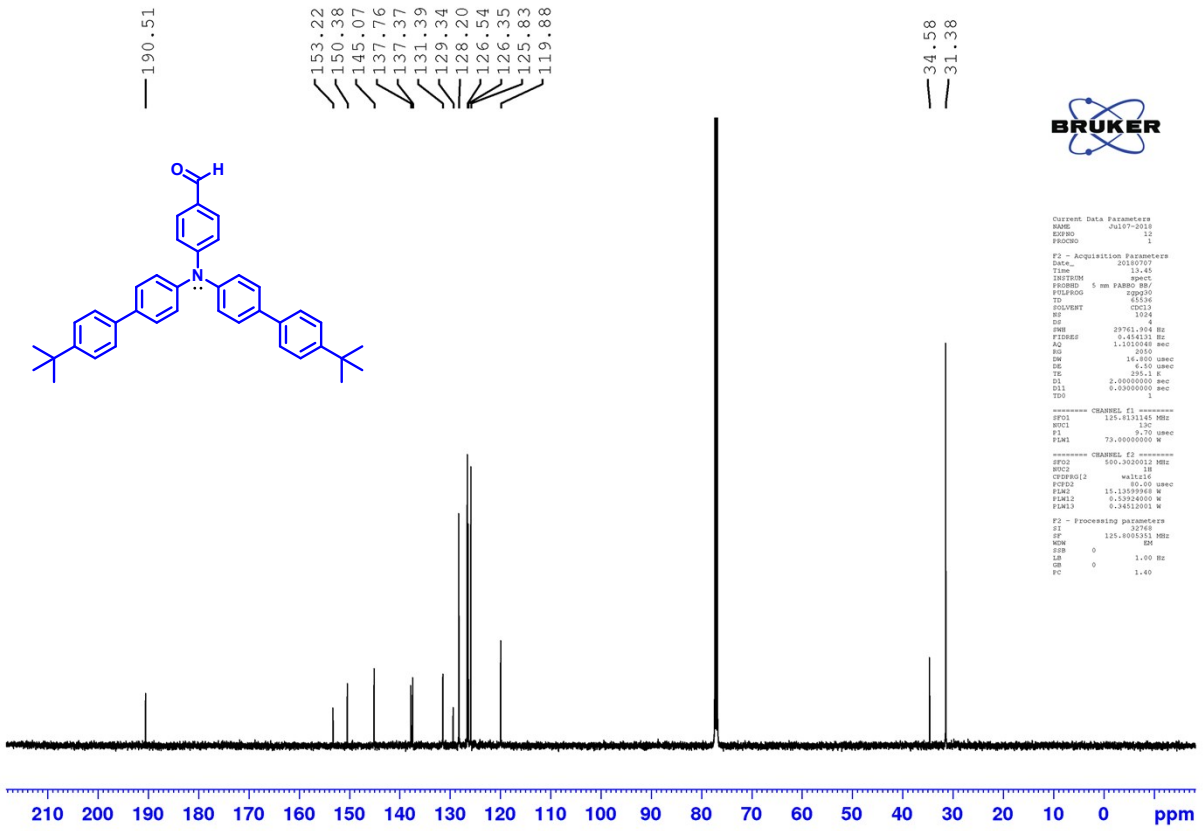

Fig. S34. ^{13}C NMR spectrum of 4-(Bis(4′-*tert*-butylbiphenyl-4-yl)amino)benzaldehyde **(3)** in $CDCl_3$.

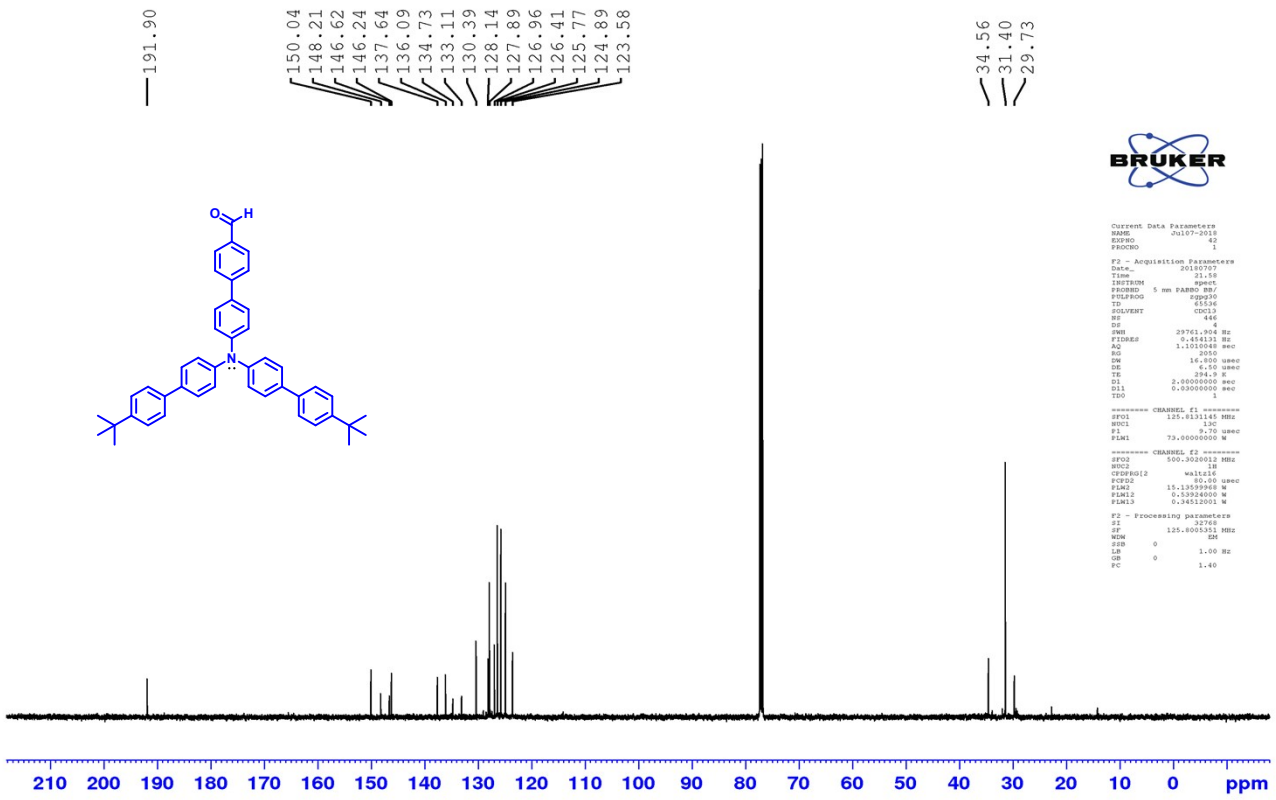

Fig. S35. ^{13}C NMR spectrum of 4′-(Bis(4′-*tert*-butylbiphenyl-4-yl)amino)biphenyl-4-carbaldehyde **(4)** in $CDCl_3$.

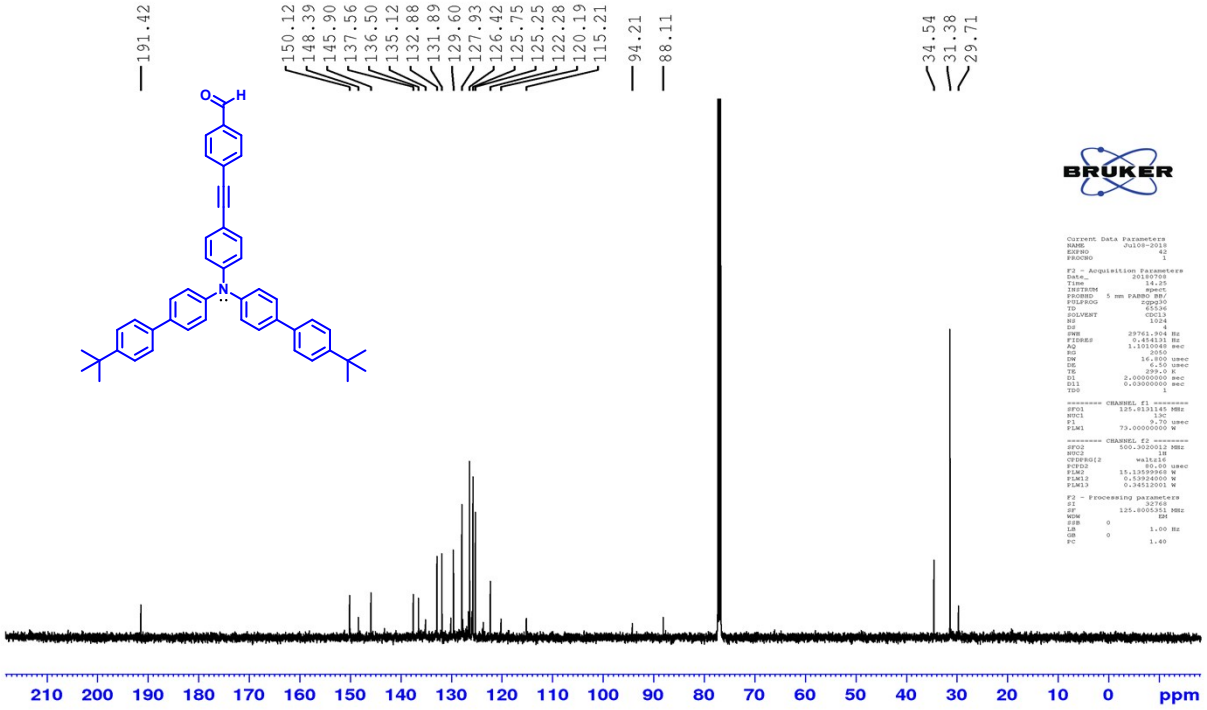

Fig. S36. ^{13}C NMR spectrum of 4-(4-(Bis (4′-*tert*-butylbiphenyl-4-yl)amino)phenylethynyl)benzaldehyde **(5)** in $CDCl_3$.

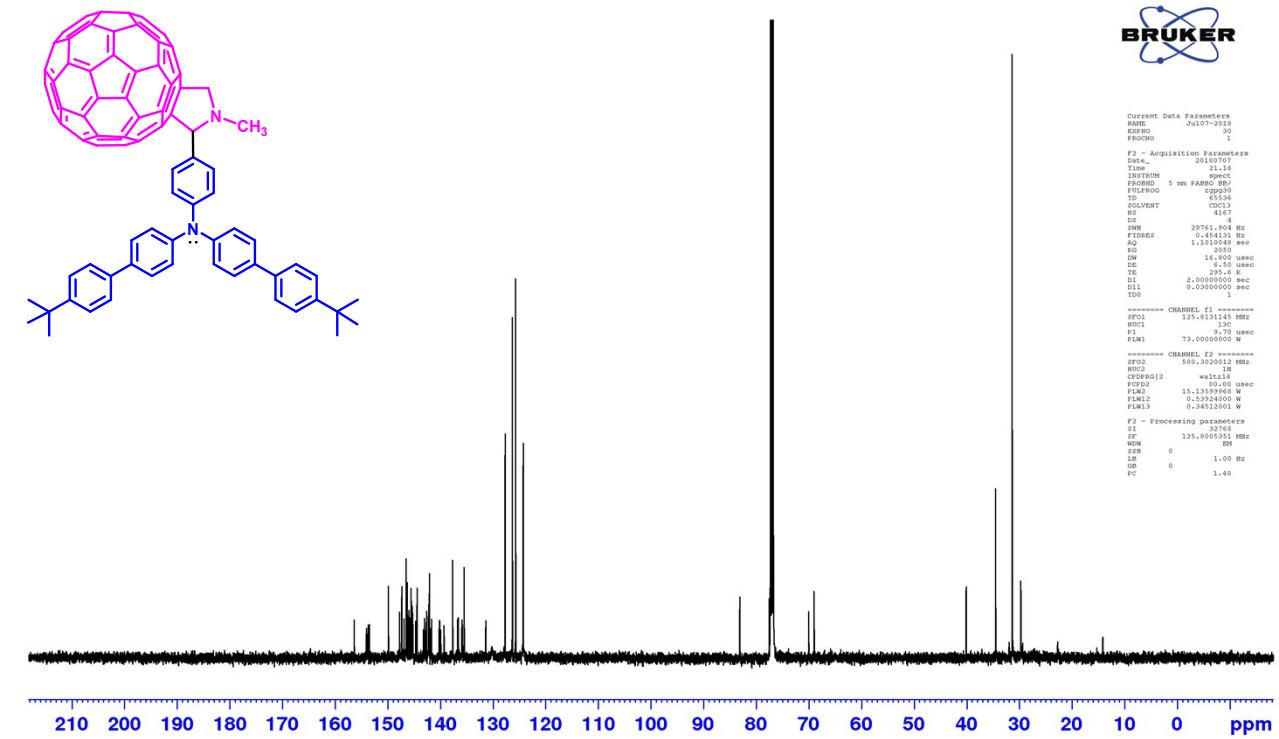

Fig. S37. ^{13}C NMR spectrum of*N*-Methyl-2-(4-(bis(4′-tert-butylbiphenyl-4-yl)amino)phenyl)-3,4-fullero[60]pyrrolidine **(6)** in $CDCl_3$

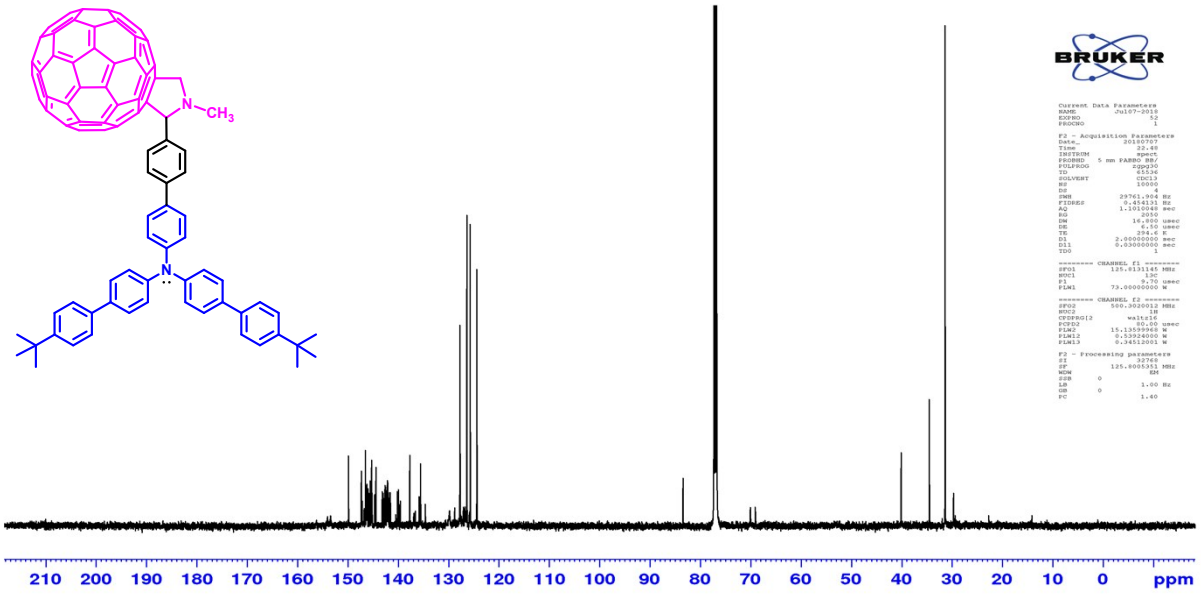

Fig. S38. ^{13}C NMR spectrum of *N*-Methyl-2-(4′-(bis(4′-*tert*-butylbiphenyl-4-yl)amino)biphenyl-4-yl)-3,4-fullero[60]pyrrolidine **(7)** in $CDCl_3$.

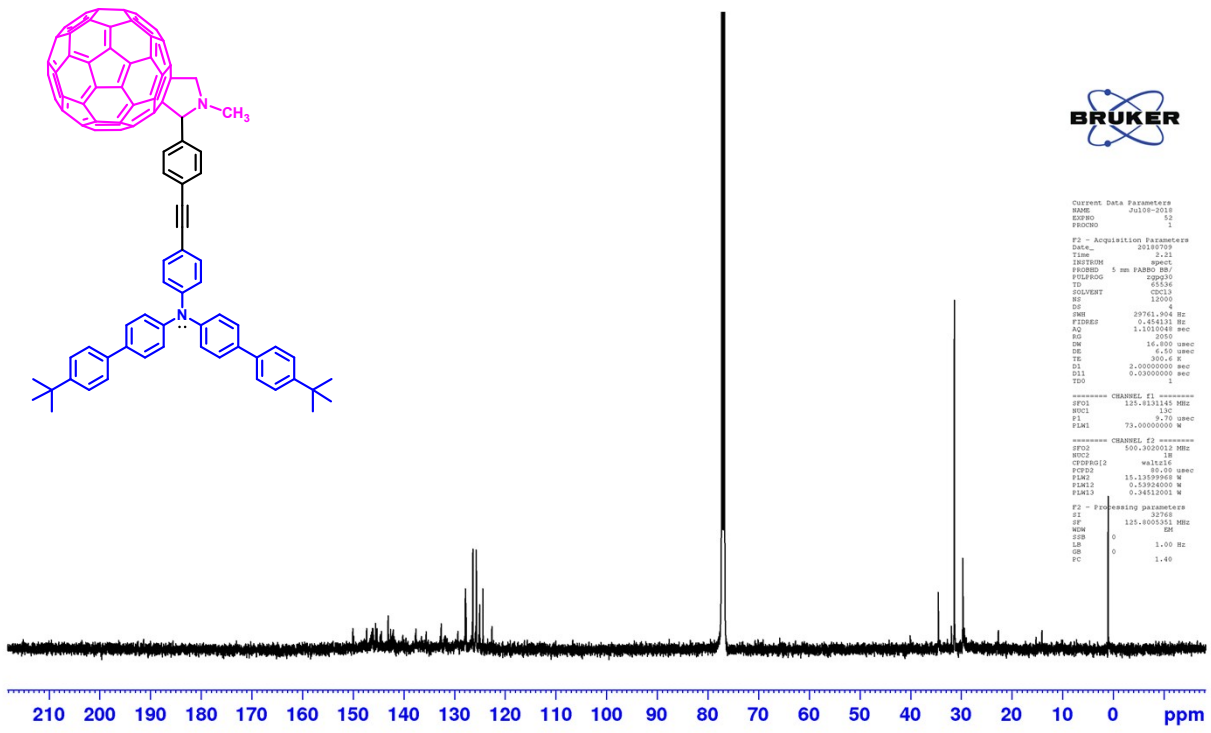

Fig. S39. ^{13}C NMR spectrum of *N*-Methyl-2-(4-(4-(bis(4′-*tert*-butylbiphenyl-4-yl)amino)phenylethynyl)phenyl-3,4-fullero[60]pyrrolidine **(8)** in $CDCl_3$.

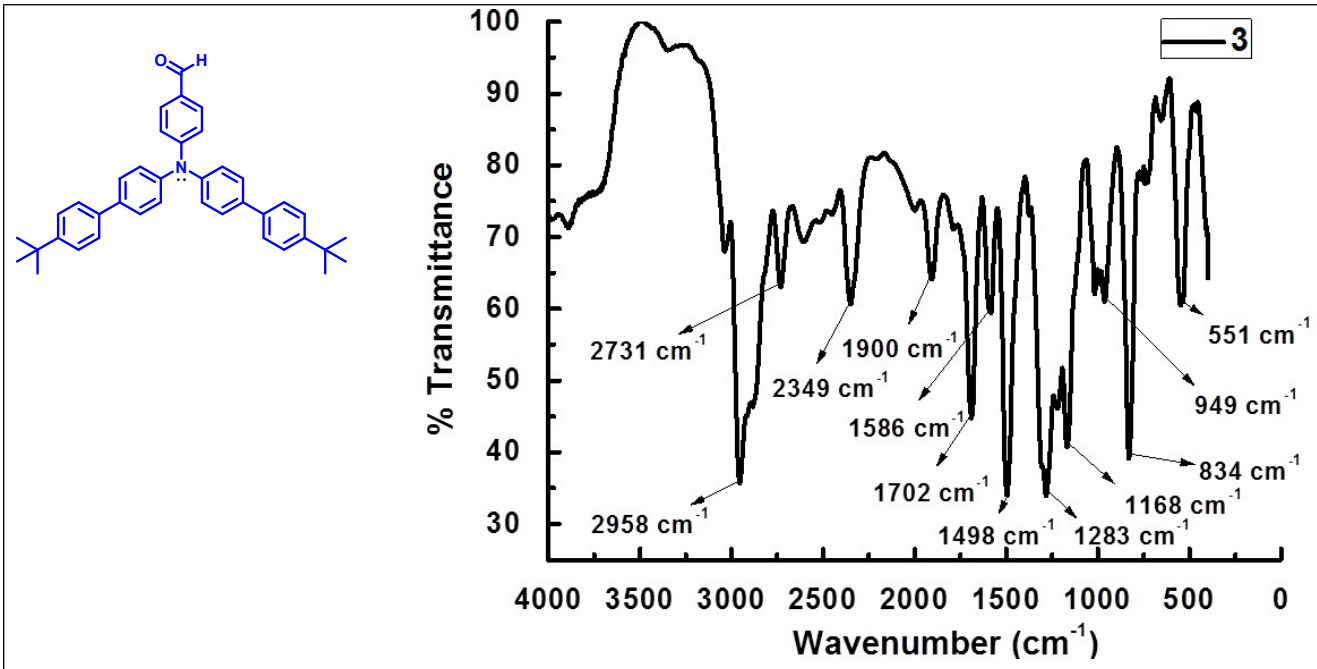

Fig. S40. FTIR spectrum of 4-(Bis(4′-*tert*-butylbiphenyl-4-yl)amino)benzaldehyde **(3)**.

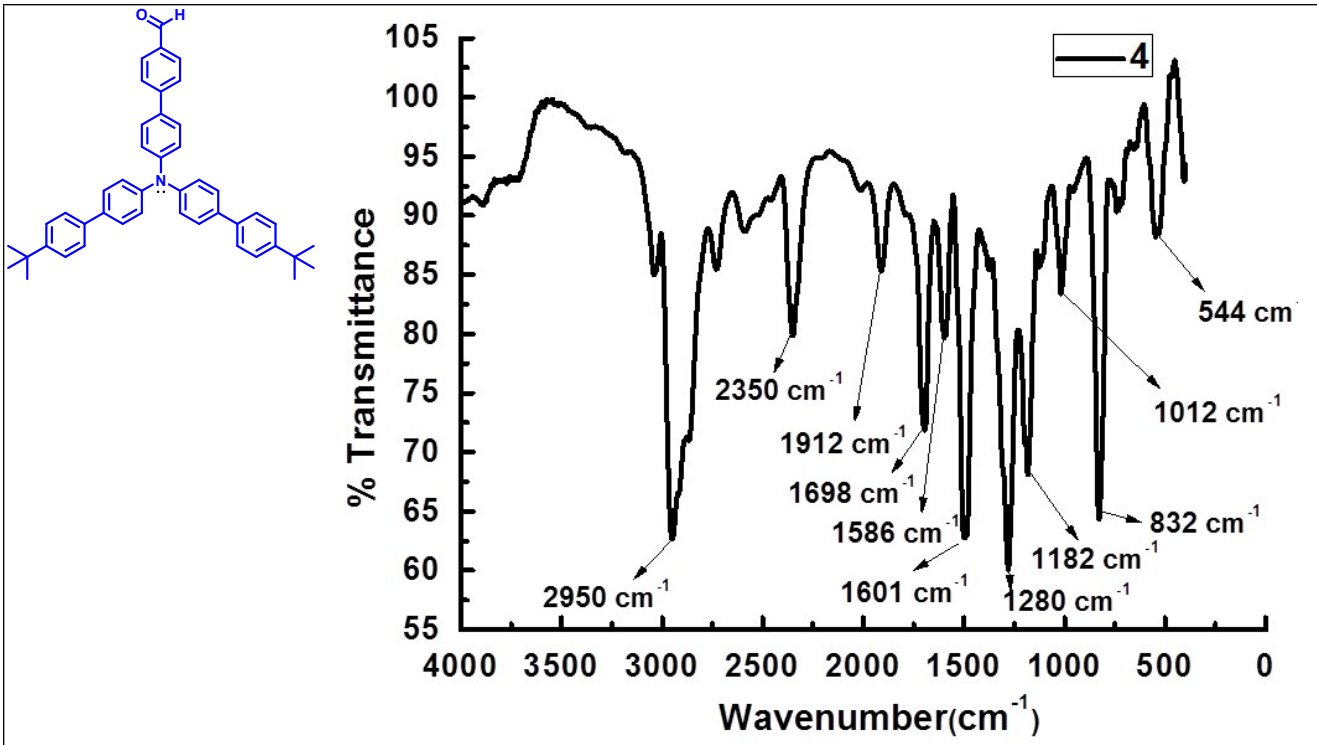

Fig. S41. FTIR spectrum of 4′-(Bis(4′-*tert*-butylbiphenyl-4-yl)amino)biphenyl-4-carbaldehyde **(4).**

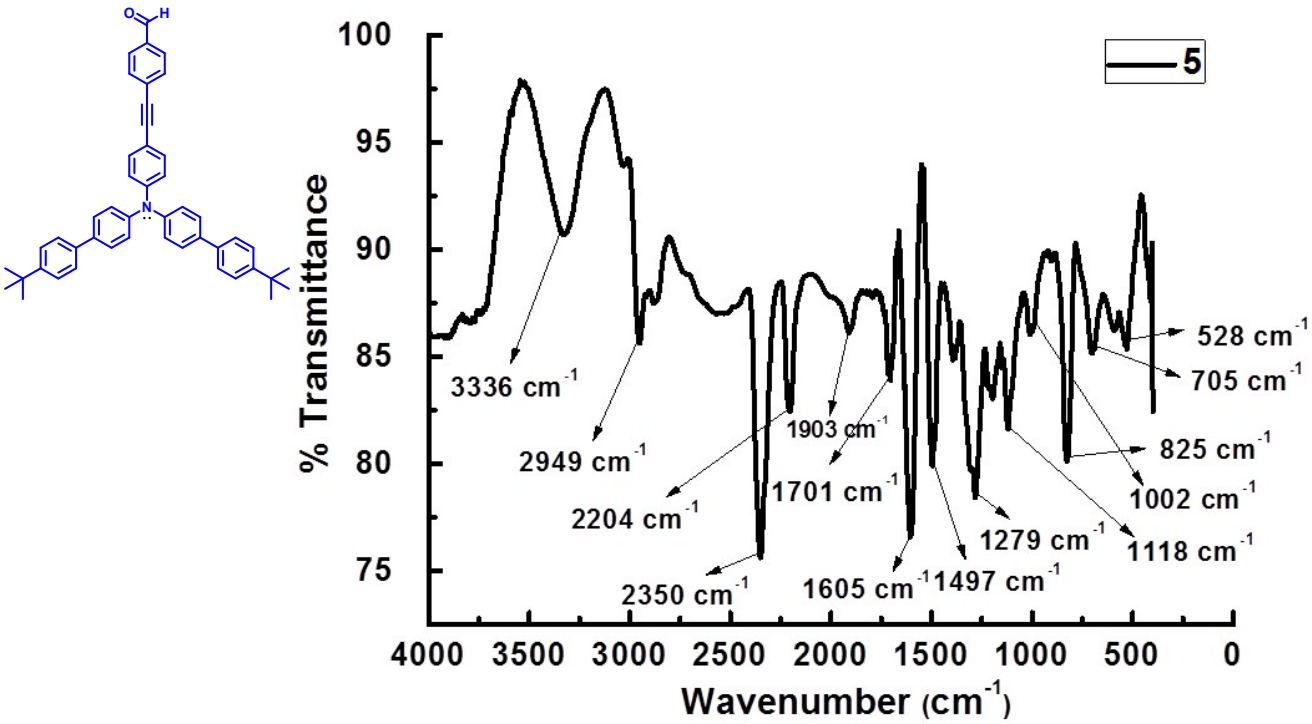

Fig. S42. FTIR spectrum of 4-(4-(Bis (4′-*tert*-butylbiphenyl-4-yl)amino)phenylethynyl)benzaldehyde **(5)**

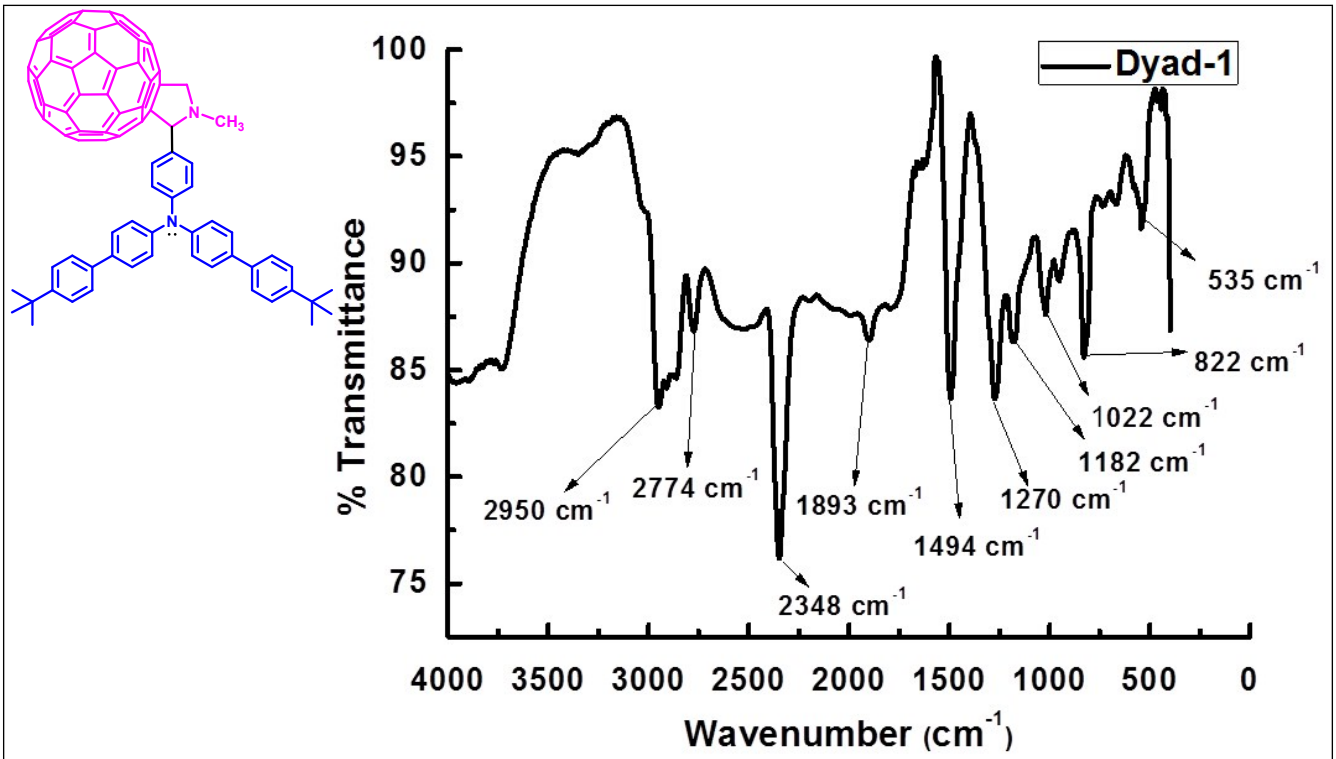

Fig. S43. FTIR spectrum of*N*-Methyl-2-(4-(bis(4′-tert-butylbiphenyl-4-yl)amino)phenyl)-3,4-fullero[60]pyrrolidine **(6)**.

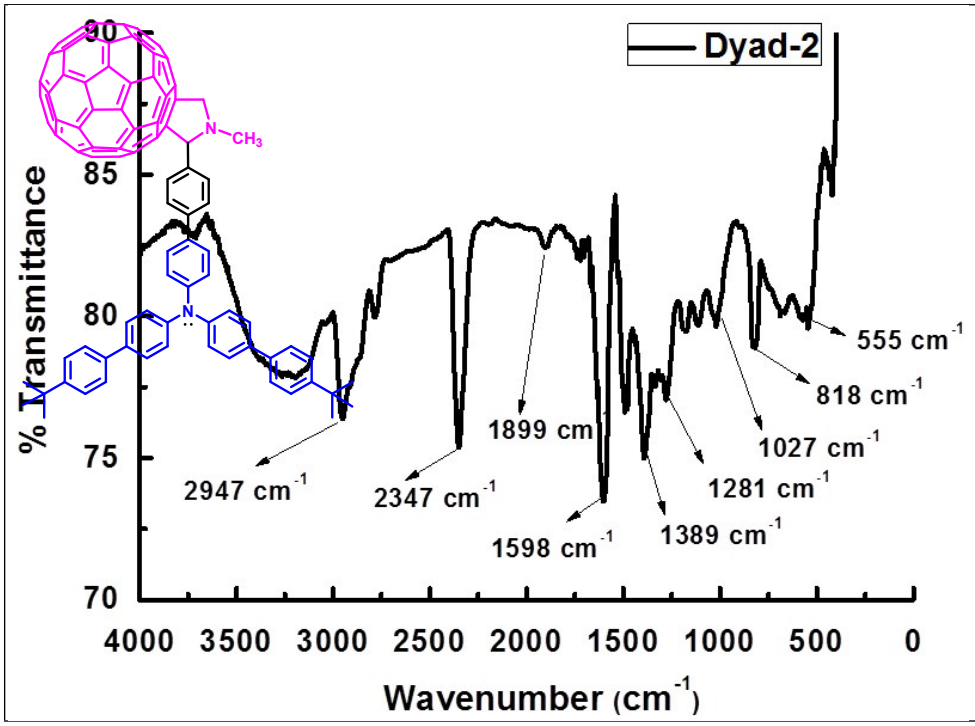

Fig. S44. FTIR spectrum of *N*-Methyl-2-(4′-(bis(4′-*tert*-butylbiphenyl-4-yl)amino)biphenyl-4-yl)-3,4-fullero[60]pyrrolidine **(7)**.

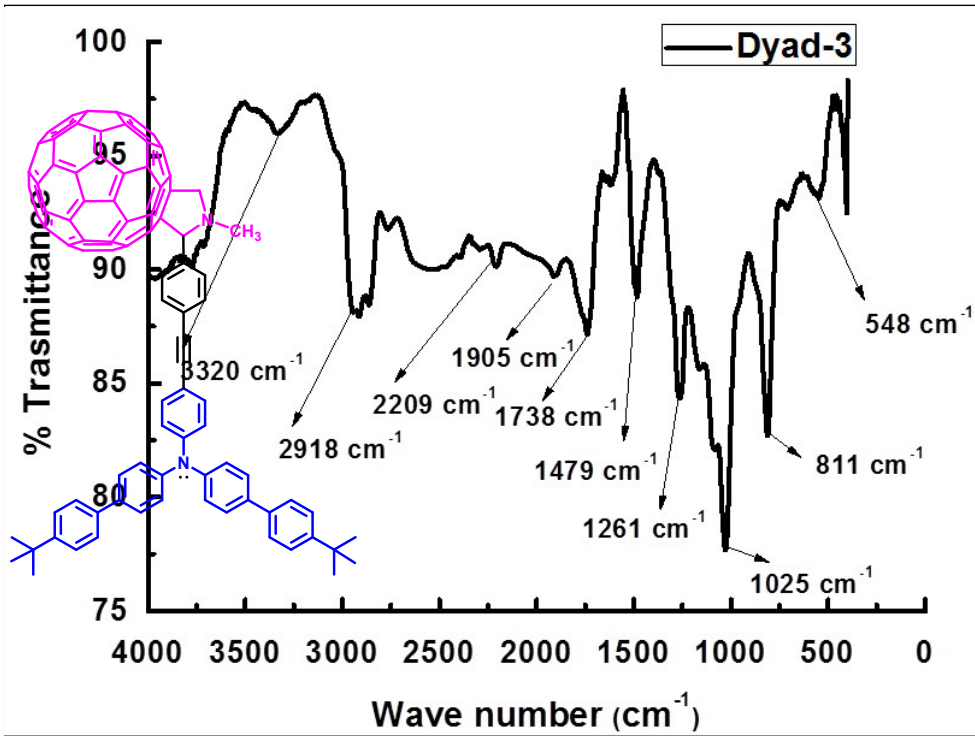

Fig. S45 FTIR spectrum of *N*-Methyl-2-(4-(4-(bis(4′-*tert*-butylbiphenyl-4-yl)amino)phenylethynyl)phenyl-3,4-fullero[60]pyrrolidine **(8)**.

References:

(1) *Gaussian 09,* Frisch, M. J.; Trucks, G. W.; Schlegel, H. B. ; Scuseria, G. E. ;Robb, M. A.; Cheeseman, J. R. ; Zakrzewski, V. G.; Montgomery, J. A.; Stratmann, R. E. ; Burant, J. C.; Dapprich, S.; Millam, J. M.; Daniels, A. D. ; Kudin, K. N. ; Strain, M. C. ; Farkas, O. ; Tomasi, J. ; Barone, V. ; Cossi, M.; Cammi, R.; Mennucci, B. ; Pomelli, C. ; Adamo, C.; Clifford, S.; Ochterski, J.; Petersson, G. A.; Ayala, P. Y.; Cui, Q.; Morokuma, K.; Malick, D. K. ; Rabuck, A. D.; Raghavachari, K.; Foresman, J. B. ; Cioslowski, J. ; Ortiz, J. V. ; Stefanov, B. B. ; Liu, G.; Liashenko, A.; Piskorz, P.; Komaromi, I.; Gomperts, R. ; Martin, R. L. ; Fox, D. J. ; Keith, T.; Al-Laham, M. A.; Peng, C. Y. ; Nanayakkara, A.; Gonzalez, C. ; Challacombe, M.; Gill, P. M. W. ;. Johnson, B. G .; Chen, W. ; Wong, M. W.; Andres, J. L.; Head-Gordon, M.; Replogle, E. S.; Pople, J. A. Gaussian, Inc., Pittsburgh, PA, 2009.

(2) Becke, A. D. *J. Chem. Phys*., **1993**, *98*, 5648–5652.

(3) Petersson, G. A.; Al-Laham, M. A. *J. Chem. Phys*. **1991**, 94, 6081.

(4) Kumar, P. H.; Venkatesh, Y.; Siva, D.; Ramakrishna, B.; Bangal, P. R. *J. Phy. Chem. A***,** **2015**, *119*, 1267.

(5) (a) Van Stokkum, I. H.; Van Oort, B.; Van Mourik, F.; Gobets, B.; Van Amerongen, H. In Biophysical techniques in photosynthesis; Springer: 2008, 223. 2. (b) Van Stokkum, I. H.; Larsen, D. S.; Grondelle, van R.; *BiochimicaBiophysicaActa(BBA)-Bioenergetics*, **2004**, *82*, 1657.

(6) (a) Laptenok, S. P.; Borst, J. W.; Mullen, K. M. ; van Stokkum, I. H.; Visser, A. J. ; Amerongen, van H.; *Phy. Chem. Chem. Phy.,***2010,***12*, 7593. (b). Mullen, K. M. ;Stokkum, Van I. H. *J. Stat. Soft.,***2007**, *18,* 1. (c) Snellenburg, J.; Laptenok, S.; Seger, R.; Mullen, K.; Van Stokkum, I.; *J. Stat. Soft.,***2012,***49,* 1. (d) MeotNer, M.; Adler, A. D. *J. Am. Chem. Soc.,***1975,** 97, 5107.